Neurobiology of Disease 148 (2021) 105184

Contents lists available at ScienceDirect

Neurobiology of Disease

journal homepage: www.elsevier.com/locate/ynbdi

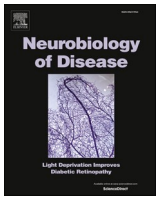

Viral-based rodent and nonhuman primate models of multiple system atrophy: Fidelity to the human disease

David J. Marmion [a,b], Angela A. Rutkowski [a], Diptaman Chatterjee [a], Benjamin M. Hiller [a], Milton H. Werner [c], Erwan Bezard [d,e], Deniz Kirik [f], Thomas McCown [g,h], Steven J. Gray [i], Jeffrey H. Kordower [a,*]

[a] Department of Neurological Sciences, Rush University Medical Center, Chicago, IL 60612, USA
[b] Parkinson's Disease Research Unit, Department of Neurobiology, Barrow Neurological Institute, Phoenix, AZ, United States
[c] Inhibikase Therapeutics, Inc., Atlanta, GA, USA
[d] University of Bordeaux, Neurodegenerative Diseases Institute, UMR 5293, F-33000 Bordeaux, France
[e] CNRS, Neurodegenerative Diseases Institute, UMR 5293, F-33000 Bordeaux, France
[f] Brain Repair and Imaging in Neural Systems (B.R.A.I.N.S) Unit, Department of Experimental Medical Science, Lund University, Lund 221 00, Sweden
[g] Gene Therapy Center, University of North Carolina, Chapel Hill, NC, USA
[h] Department of Psychiatry, University of North Carolina, Chapel Hill, NC, USA
[i] Department of Pediatrics, University of Texas Southwestern Medical Center, Dallas, TX, United States

ARTICLE INFO

Keywords:
Multiple system atrophy
Alpha synuclein
Nonhuman primate
Models
Oligodendroglia

ABSTRACT

Multiple system atrophy (MSA) is a rare and extremely debilitating progressive neurodegenerative disease characterized by variable combinations of parkinsonism, cerebellar ataxia, dysautonomia, and pyramidal dysfunction. MSA is a unique synucleinopathy, in which alpha synuclein-rich aggregates are present in the cytoplasm of oligodendroglia. The precise origin of the alpha synuclein (aSyn) found in the glial cytoplasmic inclusions (GCIs) as well the mechanisms of neurodegeneration in MSA remain unclear. Despite this fact, cell and animal models of MSA rely on oligodendroglial overexpression of aSyn. In the present study, we utilized a novel oligotrophic AAV, Olig001, to overexpress aSyn specifically in striatal oligodendrocytes of rats and nonhuman primates in an effort to further characterize our novel viral vector-mediated MSA animal models. Using two cohorts of animals with 10-fold differences in Olig001 vector titers, we show a dose-dependent formation of MSA-like pathology in rats. High titer of Olig001-aSyn in these animals were required to produce the formation of pS129+ and proteinase K resistant aSyn-rich GCIs, demyelination, and neurodegeneration. Using this knowledge, we injected high titer Olig001 in the putamen of cynomolgus macaques. After six months, histological analysis showed that oligodendroglial overexpression of aSyn resulted in the formation of hallmark GCIs throughout the putamen, demyelination, a 44% reduction of striatal neurons and a 12% loss of nigral neurons. Furthermore, a robust inflammatory response similar to MSA was produced in Olig001-aSyn NHPs, including microglial activation, astrogliosis, and a robust infiltration of T cells into the CNS. Taken together, oligodendroglial-specific viral vector-mediated overexpression of aSyn in rats and nonhuman primates faithfully reproduces many of the pathological disease hallmarks found in MSA. Future studies utilizing these large animal models of MSA would prove extremely valuable as a pre-clinical platform to test novel therapeutics that are so desperately needed for MSA.

1. Introduction

Multiple system atrophy (MSA) is a rapidly progressing neurodegenerative disorder that is extremely debilitating and fatal. MSA is devastating, but rare, with an estimated mean incidence of 0.6–0.7 cases per 100,000 person-years and increasing to 3 per 100,000 per year in the age-group above 50 years, thus classifying it as a rare disease (Bower et al., 1997). MSA affects both sexes equally, symptoms tend to emerge in the fifth to sixth decade of life (Wenning et al., 2008), and MSA progresses extremely rapidly in most cases, causing patients to be

* Corresponding author at: Department of Neurological Sciences, Rush University Medical Center, 1735 West Harrison Street, Chicago, IL 60612, USA
E-mail address: Jeffrey_kordower@rush.edu (J.H. Kordower).

https://doi.org/10.1016/j.nbd.2020.105184
Received 28 July 2020; Received in revised form 30 October 2020; Accepted 11 November 2020
Available online 19 November 2020

wheelchair bound and succumb to the disease after an average of 6–9 years following symptomatic onset (Low et al., 2015; Papapetropoulos et al., 2007; Schrag et al., 2008; Wenning et al., 2008). MSA presents clinically with varying combinations of extrapyramidal dysfunction, dysautonomia, parkinsonism, and cerebellar ataxia (Gilman et al., 2008; Low et al., 2015; Wenning et al., 2008). Based on clinical symptomatology and the distribution of pathology, MSA can be subdivided into a parkinsonian variant, MSA-P, with predominant nigrostriatal degeneration and Parkinsonian motor features, and a cerebellar variant, MSA-C, characterized by olivopontocerebellar atrophy with ataxia (Wenning et al., 2008). There are no currently available potent therapies either disease modifying or symptomatic, for MSA (Krismer and Wenning, 2017; Lopez-Cuina et al., 2018).

MSA belongs to a larger family of neurodegenerative diseases termed synucleinopathies which include Parkinson's disease (PD) and dementia with Lewy bodies (DLB), in which the protein alpha-synuclein (aSyn) forms fibrillary aggregates throughout selectively vulnerable brain regions. Synucleinopathies can be very difficult to distinguish from each other clinically, especially early in the disease process, as patients can present with overlapping symptomatology depending on the distribution of lesions or other underlying pathologies. Unlike the typical aSyn-rich neuronal aggregates found in PD and DLB, MSA is a unique synucleinopathy in which aSyn inclusions are predominantly formed in the cytoplasm of oligodendroglia (Martí et al., 2003; Papp et al., 1989). Therefore, aSyn+ glial cytoplasmic inclusions (GCIs) are the pathological hallmark of MSA and post-mortem identification of GCIs is required for a "definite" diagnosis of MSA (Gilman et al., 2008). aSyn inclusions isolated from the brains of individuals with PD, DLB, and MSA have been shown to contain structurally different aSyn filaments, and aSyn from GCIs have been reported to be three orders of magnitude more potent in seeding aggregation of aSyn than aSyn from Lewy bodies (Peng et al., 2018; Schweighauser et al., 2020). Apart from the formation of GCIs, evidence from post-mortem and experimental studies have shown that the neuropathology observed in MSA includes myelin degeneration, axonal damage, loss of neurotrophic support, neuronal degeneration, astrogliosis, microglial activation, and, recently, regional infiltration of T cells (Jellinger, 2014; Rydbirk et al., 2017; Stefanova et al., 2007; Ubhi et al., 2010; Williams et al., 2020). Subsequent studies have shown that the accumulation of GCIs seem to drive the pathology of MSA, as the degree of GCI burden strongly correlates with the level of neuronal loss and demyelination, and that the formation of GCIs occurs prior to the degeneration of axons or neurons (Ozawa et al., 2004; Papp and Lantos, 1994).

Based on the evidence linking oligodendroglial aSyn with disease pathogenesis, animal models of MSA have been developed by primarily overexpressing aSyn in oligodendrocytes via different mechanisms, variably recapitulating aspects of the disease with inherent weaknesses in each model. Transgenic (tg) mouse models have been established by genetically overexpressing human aSyn using different oligodendrocyte-specific promoters – proteolipid protein (PLP) (Kahle et al., 2002), myelin basic protein (MBP) (Shults et al., 2005), and 2′,3′-cyclic nucleotide 3′-phospho-diesterase (CNP) (Yazawa et al., 2005), or using a Cre-loxP system to express inducible oligodendroglial aSyn (Tanji et al., 2019). We and others have used viral vector-mediated overexpression of aSyn which recently has been characterized in rodents and nonhuman primates (NHPs) to produce GCIs in MSA-specific brain regions in adult animals and induce a higher level of neuropathology than tg mouse models (Bassil et al., 2017; Mandel et al., 2017; Williams et al., 2020).

In the present study, we further develop and characterize our previously established viral vector-mediated overexpression model of MSA, in which we showed 95% specificity of the novel oligotropic AAV, Olig001, to form insoluble, aSyn-rich GCIs specifically in oligodendroglia of rats and NHPs resulting in demyelination and microglial activation (Mandel et al., 2017). We now show dose-dependent myelin loss and neurodegeneration in the striatum of rats after injection of different viral titers Olig001-aSyn. Then, using the high titer Olig001-aSyn injected in the putamen of cynomolgus macaques, we demonstrate long-term robust formation GCIs and demyelination throughout its rostro-caudal putamenal extent with neuronal loss observed in both the putamen as well as the substantia nigra. Moreover, microglial activation, astrogliosis, and infiltration of T cells coincide specifically with regions of pathologic oligodendroglial-aSyn expression as we now demonstrate in human MSA samples. Our data highlights the ability of viral vector-mediated overexpression of aSyn in rats and NHPs to faithfully recapitulate many neuropathological hallmarks of MSA-P and describe a valuable large animal model to be utilized for the development of disease modifying therapies for MSA.

2. Materials and methods

2.1. Olig001 AAV vector

Detailed information of the development, construction, purification, and quality control of the Olig001 AAVs are described elsewhere (Mandel et al., 2017; Powell et al., 2016). Briefly, AAV-Olig001 vectors with a high tropism for oligodendrocytes were packaged with a self-complementary genome with transgene expression mediated by the CBh promoter and bovine growth hormone polyA (Gray et al., 2011). The AAV vectors were produced by the University of North Carolina Vector Core facility by triple-transfecting production plasmids into HEK293 cells. AAV vectors were then purified from the cells by iodixanol gradient centrifugation, followed by ion-exchange chromatography.

2.2. Rodents

Eight-week-old female Sprague-Dawley rats (Harlan, Indianapolis, IN) were used for the rodent Olig001 experiments. Upon arrival, animals were quarantined for one week prior to any testing and randomized into groups. Animals were cared for in accordance with the principles of the Guide to the Care and Use of Experimental Animals. Rats were housed two per cage with a 12:12 h light:dark cycle (07:00–19:00 h). Food and water were available ad libitum throughout the study.

2.3. Rodent stereotaxic surgery

All rats received a single 2 μl injection of Olig001 in each hemisphere at a rate of 0.5 μl/min. Rats received Olig001 in three different viral titers, 2.4×10^{11} vg/ml ($n = 8$/group), 2.3×10^{12} vg/ml (n = 8/group), and 3.72×10^{12} vg/mL ($n = 4$). The coordinates for injection were AP + 0.7 mm and ML +/− 2.7 mm from bregma, DV -5.0 mm from dura. Following the completion of each injection the micropipette was retracted 1 mm and left in place for an additional 2 min before being slowly removed from the brain. All procedures were approved by the Rush University Institutional Animal Care and Use Committee and accredited by the Association for Assessment and Accreditation of Laboratory Animal Care.

2.4. Primates

Eight adult male cynomolgus macaques (*Macaca fascicularis*) were utilized for this study and randomized to receive either Olig001-GFP or Olig001-aSyn. Animals were pair-housed on a 12-h light/12-h dark cycle. All procedures were approved by the University of Illinois Chicago Institutional Animal Care and Use Committee and the Rush University Institutional Animal Care and Use Committee and accredited by the Association for Assessment and Accreditation of Laboratory Animal Care. Animal care was supervised by veterinarians skilled in the care and maintenance of non-human primates.

2.5. Primate stereotaxic surgery

Nonhuman primates underwent surgical procedures as previously described (Mandel et al., 2017). Surgical targets were identified using pre-operative MRI and intraoperative surgical navigation using a Stealthstation Neuronavigation system. Olig001-GFP (3.75×10^{12} vg/ml) or Olig001-aSyn (3.75×10^{12} vg/ml) was injected bilaterally into the putamen (rostral putamen 20 μl, middle putamen 20 μl, caudal putamen 10 μl, 50 μl total per hemisphere) and infused at a rate of 1 μl/min.

2.6. Nonhuman primate behavior analysis

Activity Monitoring: Animals received activity monitoring to assess general motor function. Animals were fitted with a collar containing an Actical activity monitor (manufactured by Philips Respironics Murrysville, PA) which senses and records any excessive acceleration. The monitor senses acceleration that exceeds 0.05 G, recorded up to 30 times per second. The number of pulses within a pre-selected time period are then recorded. Animals were acclimated to the collars for at least 3 days prior to any data collection, recording took place for 7 days per collection interval, after which time the animals will be sedated as above and the collars were removed. Data was collected at baseline, three months post-injection, and prior to sacrifice (six months post-injection).

Fine Motor Skills Test (Hand Reach Task): Each monkey was tested for fine motor performance in both upper limbs using a hand reach task (HRT) as previously described (Emborg et al., 1998). Animals were transported to a modified testing cage from their home cage and presented with a 3 × 3 well matrix plexiglass testing board. Six pieces of food were be placed within the wells for each trial, and time will be recorded for how long it took the animal to retrieve them. The board is configured in such a manner that only one limb will be tested at a time. Monkeys underwent 10 trials per limb, with each trial being alternated between the left and right limbs. All animals were tested every two weeks by the same blinded investigator throughout the entirety of the study.

2.7. Rat and primate necropsy and tissue processing

4-weeks (rat), 5-months (rat), or 6-months (NHP) post-surgery, animals were deeply sedated and euthanized by transcardial saline perfusion. The brain was removed from the calvarium and was post-fixed in 4% paraformaldehyde solution for 12–48 h then transferred to a sucrose gradient. Coronal slices (40 μm) were sectioned on a freezing-stage sliding knife microtome and stored in cryoprotectant solution at −20 °C until processed.

2.8. Human brain samples

Post-mortem brain tissue of MSA subjects were obtained from Rush University Medical Center- approved research tissue depository with ethical approval granted by Rush University Medical Center IRB. Samples ($n = 3$) underwent a complete neuropathological evaluation confirming the presence of GCIs and diagnosis of MSA as previously described (Chu et al., 2006; Jellinger et al., 2005; Williams et al., 2020).

2.9. Immunohistochemistry

Free floating sections of brain tissue were rinsed of cryoprotectant and quenched with endogenous peroxidases using a 20-min incubation in a 0.1 M sodium periodate solution. Non-specific background staining was blocked for 1 h in 3% normal (goat or horse) serum and 2% bovine serum albumin. Sections were incubated with primary antibody (mouse anti-Living Colors JL-8 (GFP), 1:2000 dilution [632,380, Clontech]; mouse anti-tyrosine hydroxylase (TH), 1:10,000 dilution [22,941; Immunostar]; rabbit anti-Alpha-synuclein (phospho S129, EP1536Y), 1:500–1:1000 dilution [ab51253, Abcam]; mouse anti-Alpha-synuclein (LB 509), 1:500–1:1000 dilution [180,215, Thermo Fischer Scientific]; rabbit anti-Alpha-synuclein (phospho Y39), 1:100 dilution [Donated by Dr. Milton Werner]; mouse anti-NEUN (A60), 1:500 dilution [MAB 3777, EMB Millipore]; rabbit anti-Glial fibrillary acidic protein (GFAP), 1:2000 dilution [Z033401-2, Dako]; rabbit anti-CD3, 1:200 dilution [A0452, Dako];mouse anti-HLA-DR (LN3), 1:200 dilution [MA5-11966, Thermo Fischer Scientific]), 1% bovine serum albumin, 1% serum, and 0.4% Triton-X at 4 °C for 18 h. The sections were then washed, incubated with appropriate secondary antibodies (biotinylated goat anti-rabbit, 1:200 dilution [BA-1000, Vector Laboratories]; biotinylated horse anti-mouse, 1:200 dilution [BA-2000, Vector Laboratories]) for 1 h, washed again, and incubated with avidin-biotin complex (Vector Laboratories, PK-6100) for 2 h. Tissues were then incubated in imidazole-acetate buffer, pH 7.3, for 30 min before they were visualized with 3–3′-diaminobenzidine tetrahydrochloride in 0.01% hydrogen peroxide with 2% nickel enhancement. The sections were allowed to dry overnight, dehydrated through increasing alcohol concentrations and xylenes, and coverslipped with cytoseal (23,244,257; Fisher Scientific International).

2.10. Immunofluorescence double labeling

Free floating sections of brain tissue were rinsed of cryoprotectant and non-specific background staining was blocked for 1 h in 3% normal (goat) serum and 2% bovine serum albumin. Sections were incubated with primary antibody (mouse anti-Living Colors JL-8 (GFP), 1:2000 dilution [632,380; Clontech]; mouse anti-tyrosine hydroxylase (TH), 1:10,000 dilution [22,941; Immunostar]; rabbit anti-tyrosine hydroxylase (TH), 1:3000 dilution [AB152; EMB Millipore]; mouse anti-Alpha-synuclein (LB 509), 1:500–1:1000 dilution [180,215; Thermo Fischer Scientific]; rabbit anti-Alpha-synuclein (phospho S129, EP1536Y), 1:500–1:1000 dilution [ab51253, Abcam]; rabbit anti-alpha synuclein (rodent specific, D37A6), 1:500 dilution [4179S; Cell Signaling]; rabbit anti-p25α, 1:500 dilution [generously donated by Dr. Poul Henning Jensen]; rabbit anti-Olig2 [EPR2673], 1:200 dilution [ab109186; Abcam]), 1% bovine serum albumin, 1% serum, and 0.4% Triton-X at 4 °C for 18 h. The sections were then washed, incubated with appropriate secondary antibodies (Alexa Fluor® 488 AffiniPure Goat Anti-Mouse IgG, 1:200 [115–545-003; Jackson Immuno Research Laboratories]; Alexa Fluor® 647 AffiniPure Fab Fragment Goat Anti-Mouse IgG, 1:200 [115–607-003; Jackson Immuno Research Laboratories]; Alexa Fluor® 488 AffiniPure Goat Anti-Rabbit IgG, 1:200 dilution [111–545-003; Jackson Immuno Research Laboratories]; Alexa Fluor® 647 AffiniPure Goat Anti-Rabbit IgG, 1:200 dilution [111–605-003; Jackson Immuno Research Laboratories]) for 1 h, washed again, and mounted on glass slides. The sections were allowed to dry overnight, dehydrated through increasing alcohol concentrations and xylenes, and coverslipped with DPX mounting medium (Sigma, 44,581).

2.11. Proteinase K digestion

Proteinase K (PK) digestion was used to determine whether the aSyn seen in oligodendrocytes was soluble (non-aggregated) or insoluble (aggregated), the remaining signal detecting the later. Striatal sections containing the injection site were mounted onto gelatin-coated slides and dried for at least 8 h at 55 °C. After wetting with TBS-T (10 mM Tris–HCl, pH 7.8; 100 mM NaCl; 0.05% Tween-20), the sections were digested with 10 μg/ml PK (Invitrogen) in TBS-T (10 mM Tris–HCl, pH 7.8; 100 mM NaCl; 0.1% Tween-20) for 30 min at 55 °C. The sections were fixed with 4% paraformaldehyde for 10 min. After several washes, the sections were processed for anti-Alpha-synuclein (LB509) IHC as described (Mandel et al., 2017).

2.12. Luxol fast blue

For analysis of myelin integrity, level matched sections of both Olig001-GFP and Olig001-aSyn injected rats and monkeys were mounted on glass slides and allowed to dry overnight. Sections were placed in a 1:1 alcohol/chloroform solution to defat the tissue, rinsed in 70% alcohol, and placed in a 0.1% Luxol Fast Blue solution overnight at 56 °C. Sections were destained using 0.05% lithium carbonate solution and 70% alcohol until gray matter was clear and white matter was clearly defined.

2.13. Stereology

Unbiased stereological counting methods (West and Gundersen, 1990) using the Stereo Investigator optical fractionator probe (Microbrightfield Bioscience, Version10.40) were utilized to assess the number of GCIs, neuronal degeneration, and T cell populations in Olig001 injected rats and NHPs. Briefly, the region of interest was outlined at 1.25× magnification and a systematic sampling of serial sections was employed where cells were counted using a 60× oil-immersion objective from a random starting point at regular predetermined intervals. Details for specific counting parameters are found in Supplemental Table 1.

2.14. Optical density

Eight level matched serial sections of Olig001 injected monkeys stained for HLA-DR and GFAP were used in these analyses. The putamen was imaged using 4× objective on a Nikon eclipse Ti2 microscope using a Nikon D5-Ri2 colour camera and NIS elements AR software version 5.10.01. Quantified images were all taken with identical acquisition settings. The acquired image files were analyzed by a blinded rater and quantified with mean gray value units using imageJ (NIH) software. Briefly, the region of interest was outlined and converted to gray scale. The image was then inverted, vessels and holes in the tissue were excluded, and the background was subtracted using rolling ball radius of 25 prior to data collection.

2.15. In situ hybridization

A combination of in situ hybridization (ISH) for Olig001 and IHC of either Olig2 or NeuN using RNAscope® (Advanced Cell Diagnostics) to determine the cellular specificity of the Olig001 AAV as previously described (Grabinski et al., 2015; Wang et al., 2012). The ISH probe was designed to recognize the non-transcribed region within the promoter region of Olig001. The ISH signal was detected using 3, 3′-diaminobenzidine to produce brown punctate staining. Following RNAscope ISH labeling, the sections were processed for either Olig2 or NeuN IHC (as described above) using Vector slate-gray to produce blue-gray labeling of oligodendrocytes or neurons.

2.16. Thioflavin S

Thioflavin S histochemistry was performed to determine whether aSyn antibody-labeled inclusions contained amyloid fibrils with beta-pleated sheet structures analogous to pathology in human synucleinopathies. Striatal sections of Olig001-aSyn NHPs were mounted on gelatin-coated slides and dried at room temperature. Mounted sections were defatted in equal parts of chloroform and 100% ethanol for 2 h and stained with 0.1% thioflavin S for 10 min in the dark (Kordower et al., 2008).

2.17. Images

Confocal images were obtained from either an Olympus laser-scanning microscope with Fluoview software or a Nikon Eclipse Ti2 confocal microscope using a Nikon A1RHD camera using NIS elements AR software version 5.10.01 and stored as tiff files. Conventional light microscopic images were acquired using an Olympus microscope (BX61) attached to a Nikon digital camera DXM1200 or a Nikon eclipse Ti2 microscope using a Nikon D5-Ri2 colour camera and NIS elements AR software version 5.10.01. All compared images were taken using the same intensity and exposure time. All figures were prepared using Photoshop 8.0 graphics software. Only minor adjustments of brightness or contrast were made.

3. Statistical analyses

All data are presented as mean ± SEM. All statistical tests were conducted using GraphPad Prism 8 software. The specific statistical test and statistical details for individual experiments can be found in the corresponding figure legends.

4. Data availability

The data that support the findings of this study are available from the corresponding author, upon reasonable request.

5. Results

5.1. Olig001 titer comparison, GCI formation, and neuronal loss in rats

To investigate the dose dependency of aSyn overexpression in oligodendrocytes, two titers of AAV Olig001 were injected in the striatum of Sprague Dawley rats. Five months following injection, the rats were sacrificed and transduction of oligodendroglia was evaluated by histological analysis. GFP expression was observed in oligodendroglia throughout the striatum and corpus callosum (CC) of Olig001-GFP injected rats (Fig. 1a, a′, 2.4×10^{11}–2.3×10^{12} vg/ml), however aSyn transgene expression greatly differed between low titer (LT) (Fig. 1b, b′, 2.4×10^{11} vg/ml) and high titer (HT) (Fig. 1c, c′, 2.3×10^{12} vg/ml) Olig001-aSyn injected animals using human aSyn (LB509, Supplementary Fig. 1) and pathological, phosphorylated Serine-129 (pS129) aSyn antibodies. In LT Olig001-aSyn injected rats, sparse aSyn+ inclusions were seen around the needle tract in the striatum (Fig. 1b, b′), while widespread, prominent aSyn+ inclusions were seen throughout the CC and abundant in white matter bundles throughout the striatum in HT Olig001-aSyn injected rats (Fig. 1c, c′). Human-specific aSyn immunoreactivity (LB509) was also observed in other structures such as the globus pallidus, thalamus, and substantia nigra (Supplementary Fig. 1a–d). Unbiased stereological counts of pS129 aSyn+ inclusions in the striatum showed a significant 210% increase in HT titer aSyn injected animals compared to LT animals (Fig. 1d, HT Olig001-aSyn: 23,828 ± 2455; LT Olig001-aSyn: 7662 ± 2074, $^{**}P \leq 0.01$).

The extent and localization of aSyn-rich GCIs has been shown to be highly correlative with the degree of neuronal loss and demyelination in post-mortem human MSA cases (Ozawa et al., 2004; Papp et al., 1989). Therefore, we sought to investigate if this aspect of the disease was recapitulated in the novel Olig001 MSA rat model and if differences in AAV titer influenced the observed neuropathology. In order to investigate the degree of neuronal loss, rat brain sections were stained for neuronal marker NeuN and evaluated using unbiased stereology in the striatum. Corresponding with aSyn pathology, a titer-dependent loss of NeuN+ striatal neurons was found in LT Olig001-aSyn (14.7%) and HT Olig001-aSyn (23.8%) groups compared to Olig001-GFP injected rats (Fig. 1e, LT Olig001-aSyn: 116,407 ± 1945; HT Olig001-aSyn: 104,035 ± 5484; Olig001-GFP: 136,500 ± 6247, Tukey's multiple comparison GFP vs LT aSyn: $^{*}P \leq 0.05$; GFP vs HT aSyn: $^{***}P \leq 0.001$; LT aSyn vs HT aSyn: ns). As neuronal loss is also observed in the substantia nigra of subjects with MSA, nigral sections of Olig001-injected rats were stained with dopaminergic marker tyrosine hydroxylase (TH). Similar to striatal neurodegeneration, unbiased stereological counting revealed a titer-dependent loss of TH+ neurons in LT Olig001-aSyn (21.7%) and HT

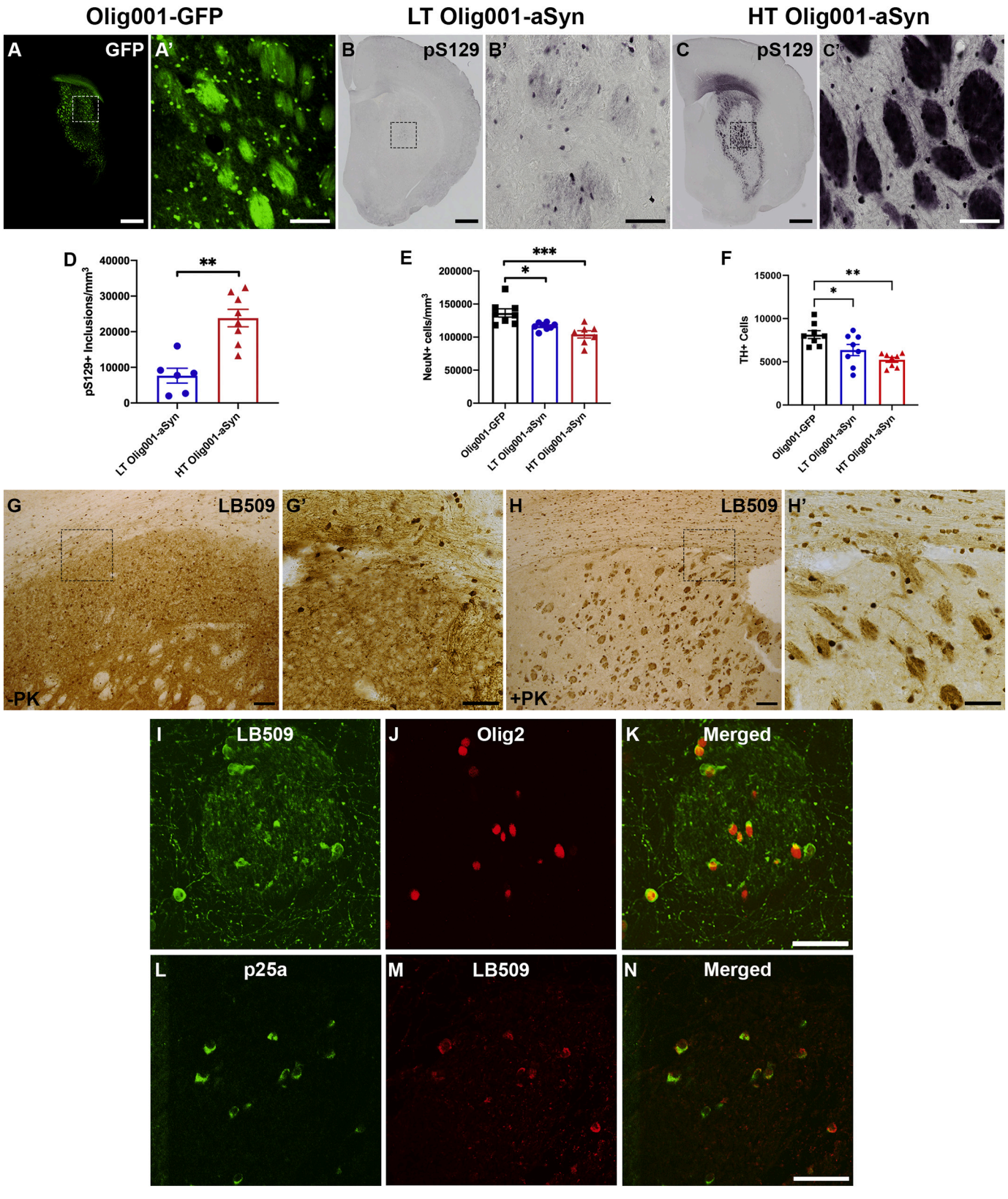

(caption on next page)

Fig. 1. Olig001 transduction of rat striatal oligodendrocytes. Representative photomicrographs of striatum of rats injected with Olig001-GFP (a and a′), LT Olig001-aSyn (b and b'), and HT Olig001-aSyn (c and c') illustrating oligodendroglial transduction of transgene. Scale bars: a, b, and c = 1000 μm; a′, b′, and c = 50 μm. Stereological analysis (d) revealed a significant 210% increase in the density of pS129+ inclusions in HT Olig001-aSyn injected animals compared to LT Olig001-aSyn (HT Olig001-aSyn: 23,828 ± 2455; LT Olig001-aSyn: 7662 ± 2074, $^{**}P \leq 0.01$, Two-tailed Mann Whitney Test, $n = 8$/group). Stereological analysis (e) revealed a titer-dependent loss of striatal NeuN+ neurons was found in LT Olig001-aSyn and HT Olig001-aSyn groups compared to Olig001-GFP injected rats (LT Olig001-aSyn: 116,407 ± 1945; HT Olig001-aSyn: 104,035 ± 5484; Olig001-GFP: 136,500 ± 6247, Tukey's multiple comparison GFP vs LT aSyn: $^{*}P \leq 0.05$; GFP vs HT aSyn: $^{***}P \leq 0.001$ LT aSyn vs HT aSyn: ns, n = 8/group). Stereological analysis (f) revealed a titer-dependent loss of nigral TH+ neurons was found in LT Olig001-aSyn and HT Olig001-aSyn groups compared to Olig001-GFP injected rats (LT Olig001-aSyn: 6372 ± 651.6; HT Olig001-aSyn: 5222 ± 279.8; Olig001-GFP: 8148 ± 456.9, Tukey's multiple comparison GFP vs LT aSyn: $^{*}P \leq 0.033$; GFP vs HT aSyn: $^{**}P \leq 0.002$ LT aSyn vs HT aSyn: ns, n = 8/group). LB509 aSyn stained Olig001-aSyn sections without (g and g') and with PK digestion (h and h') illustrating insoluble aSyn aggregates. Scale bars: g and h = 100 μm, g' and h' = 10 μm. Confocal microscopy of HT Olig001-aSyn injected animals illustrates LB509+ aSyn staining (i and k, green) surrounding the nuclear oligodendroglial Olig2+ signal (j and k, red) confirms the cytoplasmic location of the aSyn aggregates in the cytoplasm of oligodendrocytes. Scale bar: e-g = 50 μm. Confocal microscopy of HT Olig001-aSyn injected animals illustrates the co-localization of microtubule stabilizing protein p25α (l and n, green) with LB509+ aSyn inclusions (m and n, red) in the cytoplasm of oligodendroglia. Scale bar: j-l = 50 μm. (For interpretation of the references to colour in this figure legend, the reader is referred to the web version of this article.)

Olig001-aSyn (35.9%) groups compared to Olig001-GFP injected rats (Fig. 1f, LT Olig001-aSyn: 6372 ± 651.6; HT Olig001-aSyn: 5222 ± 279.8; Olig001-GFP: 8148 ± 456.9, Tukey's multiple comparison GFP vs LT aSyn: $^{*}P < 0.033$; GFP vs HT aSyn: $^{**}P < 0.002$; LT aSyn vs HT aSyn: ns).

GCIs composed of insoluble aSyn aggregates are critical MSA hallmarks to replicate within a relevant disease model. To evaluate the solubility of aggregates within GCIs in the Olig001-aSyn MSA rat model, striatal sections of Olig001-aSyn injected rats were subjected to proteinase-K (PK) digestion followed by human-specific LB509 aSyn staining. Striatal sections without PK treatment displayed robust LB509+ aggregates throughout the CC and striatum as well as granular LB509+ staining in oligodendrocytes processes (Fig. 1g and g′). Following PK digestion, much of the LB509+ staining in the processes degraded, while substantial staining of the LB509+ aggregates in the oligodendroglia remained (Fig. 1h and h′), indicating the formation insoluble aSyn rich aggregates in the Olig001-aSyn MSA rat model, similar to clinical MSA. The use of HT Olig001-aSyn did not result in off-target transduction and remained oligotropic, as human-specific LB509+ aSyn aggregates (Fig. 1i, green) are shown surrounding the nuclear signal of oligodendroglial marker Olig2 (Fig. 1j, red), confirming the cytoplasmic localization of aSyn and formation of GCI-like aSyn rich inclusions (Fig. 1k). Double staining utilizing human-specific aSyn antibody LB509 with pS129 aSyn antibody (Supplementary Fig. 2a–c) and human-specific aSyn antibody LB509 with rodent-specific aSyn antibody D37A6 (Supplementary Fig. 2d–f) indicates that exogenously expressed human aSyn is phosphorylated at serine 129, while endogenous rodent aSyn is not a component of the GCI-like formations.

Under physiological conditions, the oligodendroglia-specific phosphoprotein p25α/tubulin polymerization promoting protein (TPPP) is found in the nucleus and myelin sheath where it interacts with myelin basic protein (MBP) and tubulin to facilitate myelination and the stabilization of microtubules. In human MSA, it has been shown that p25α relocates to the cytoplasm of oligodendroglia early in the disease course where it is involved in the recruitment of aSyn to form GCIs and is another major component of GCIs (Mavroeidi et al., 2019; Ota et al., 2014). Immunofluorescent double labeling revealed that p25α (Fig. 1l, green) co-localized with LB509+ aSyn aggregates (Fig. 1m, red) following Olig001-aSyn injection, replicating the presence of p25α in GCIs of clinical MSA.

5.2. aSyn overexpression destabilizes myelin

Since the relocation of p25α to the cytoplasm destabilizes myelin, Luxol Fast Blue (LFB) staining and electron microscopy (EM) were used to evaluate the myelin integrity. Regions of pS129+ aSyn staining in the striatum of HT Olig001-aSyn rats (Fig. 2a) displayed robust demyelination of striosomes as shown by decreased LFB staining in level matched sections (Fig. 2b, arrowheads). In contrast, Olig001-GFP injected rats displayed oligodendroglial tropism (Fig. 2c) but no demyelination (Fig. 2d). Furthermore, EM of striatal sections of Olig001-aSyn injected rats showed atypical myelination (Fig. 2e, red arrows), where the myelin sheath became unraveled when compared to tightly-wound pattern of myelination observed around unaffected, neighboring axons (Fig. 2e, black arrow). Taken together, these results show that a higher titer of Olig001-aSyn elicits strong MSA-like pathology with respect to oligodendroglial function.

5.3. Oligodendrocyte-to-neuron transfer of aSyn in substantia Nigra

In the HT Olig001-aSyn injected group, aSyn+ aggregates were seen in the substantia nigra (Fig. 3a, a′), as well as in the globus pallidus and thalamus (Supplementary Fig. 1). To determine if the pS129+ inclusions found in nigral neurons was a result of neuronal uptake of the Olig001 AAV or "transport" of aSyn, RNAscope® in situ hybridization was performed using a probe specific to a non-transcribed region within the promoter region of Olig001, followed by immunohistochemistry to detect either neurons or oligodendroglia. Positive staining of the RNAscope® probe (Fig. 3b, brown staining) was seen to co-localize with oligodendrocyte marker Olig2 (Fig. 3b, blue staining) in the substantia nigra. Positive staining of the RNAscope® probe was not observed within NeuN+ neurons in the substantia nigra (not shown), indicating that the neurons that contained pS129+ inclusions did not uptake the Olig001-aSyn vector, but suggests limited oligodendrocyte-to-neuron "transfer" of aSyn in this model. Immunofluorescent double labeling showed that the pS129+ aggregates (Fig. 3c, green) co-localized with tyrosine hydroxylase+ (TH+) neurons (Fig. 3d, e, red), indicating aSyn uptake specifically in dopamine neurons of the substantia nigra. Stereological counting of TH+ neurons and pS129+ aggregates indicate that 11% of TH+ neurons contained pS129+ inclusions. Human-specific LB509 aSyn immunoreactivity in TH+ nigral neurons (Fig. 3f–h) indicates exogenous accumulation of vector-derived aSyn, while the lack of colocalization with rodent-specific aSyn and TH rules out the recruitment of endogenous rat aSyn (Fig. 3i–k).

5.4. GCI formation in Olig001 injected NHPs

Using the high-titer of Olig001 dose that yielded more pronounced MSA-like pathology, cynomolgus macaques received three injections bilaterally in the putamen of either Olig001-aSyn or Olig001-GFP ($n = 4$ per group). Six months post-injection, all monkeys showed remarkable transgene expression. Extensive LB509+ aSyn immunoreactivity was observed throughout the rostral-caudal extent of the putamen in Olig001-aSyn NHPs and displays the classical morphology of GCIs in clinical MSA (Fig. 4a, a′). Double staining using LB509 and Olig2 displayed the specific cytoplasmic localization of aSyn in oligodendroglia in Olig001-aSyn injected NHPs (Fig. 4b–d). Increasing evidence has shown elevated levels of the tyrosine kinase c-Abl in PD (Brahmachari et al., 2016; Brahmachari et al., 2019; Imam et al., 2011; Ko et al., 2010; Mahul-Mellier et al., 2014) and other neurodegenerative diseases

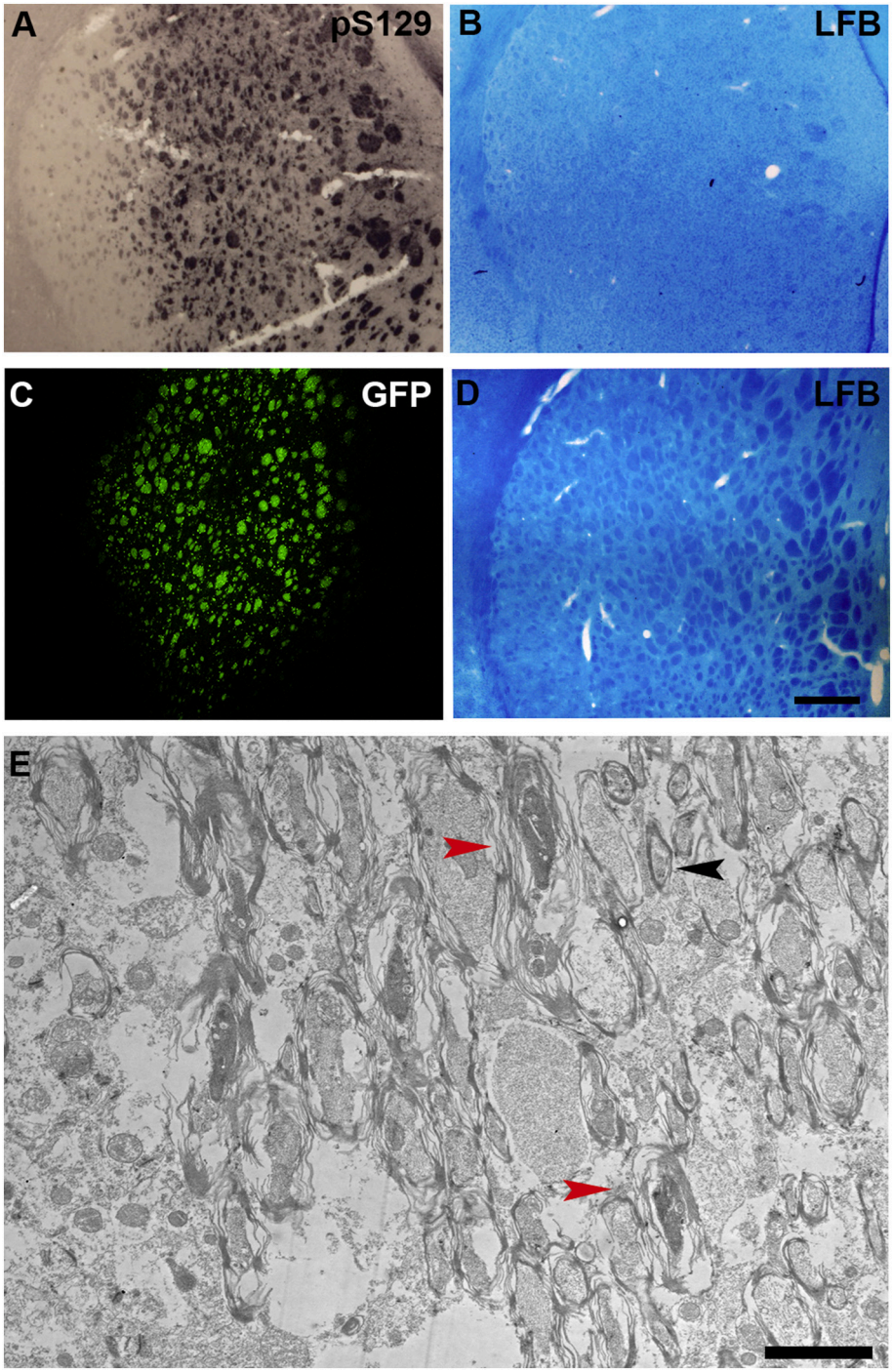

Fig. 2. aSyn induced myelin disorganization in rats. Photomicrograph of pS129 aSyn immunoreactivity in Olig001-aSyn injected rats (a) correspond to regions of demyelination in level matched sections shown by loss of LFB staining (b). GFP expression in Olig001-GFP rats (c) does not induce demyelination (d) n = 8/group. Scale bars: a-d = 500 μm. LFB = Luxol Fast Blue. Electron microscopy image of Olig001-aSyn injected rat striatum (e). Red arrowheads denote unwound myelin sheath, black arrowheads denote few remaining intact myelin sheaths. Scale bar: 2 μm. *N* = 4. (For interpretation of the references to colour in this figure legend, the reader is referred to the web version of this article.)

(Alvarez et al., 2008; Cancino et al., 2008; Jing et al., 2009; Schlatterer et al., 2011; Tremblay et al., 2010). In PD, c-Abl has been found to phosphorylate parkin, which inhibits the ubiquitin ligase activity and neuroprotective functions of parkin, and aSyn has been identified as a substrate for c-Abl and catalyzes the phosphorylation of aSyn at tyrosine 39 (pY39), whereby pY39 increases aSyn's propensity to aggregate (Brahmachari et al., 2016; Brahmachari et al., 2019; Hebron et al., 2013; Mahul-Mellier et al., 2014). To investigate if this pathologic post-translational modification of aSyn is present in MSA, post-mortem brain sections from pathologically confirmed MSA cases were immunostained using antibodies specific to pS129 and pY39 motifs on aSyn. Widespread staining of pS129 and pY39 aSyn+ GCIs was observed throughout the putamen (Fig. 4e and h) and substantia nigra (Fig. 4f and i) of post-mortem MSA cases. Similar staining patterns for pS129 and pY39 were seen in the striatum of Olig001-aSyn injected NHPs (Fig. 4g and j), indicating that c-Abl-mediated phosphorylation occurs in MSA as well as PD. Unbiased stereological counts in the region of transduction demonstrated that no significant differences were observed between the number of GFP+ or aSyn+ cells, indicating that the specific accumulation of aSyn specifically, not the number of transduced cells, is responsible for any observed pathology (Fig. 4k, Olig001-GFP NHPs: 25,529 ± 3758 GFP+ cells/mm^3; Olig001-aSyn NHPs: 28,830 ± 1410 LB509+ cells/mm^3 and 34,162 ± 6161 pS129+ cells/mm^3). Furthermore, striatal sections from Olig001-aSyn injected NHPs contain GCIs that stain positive for Thioflavin S (Fig. 4l), indicating the formation of beta-pleated sheets akin to GCIs in MSA.

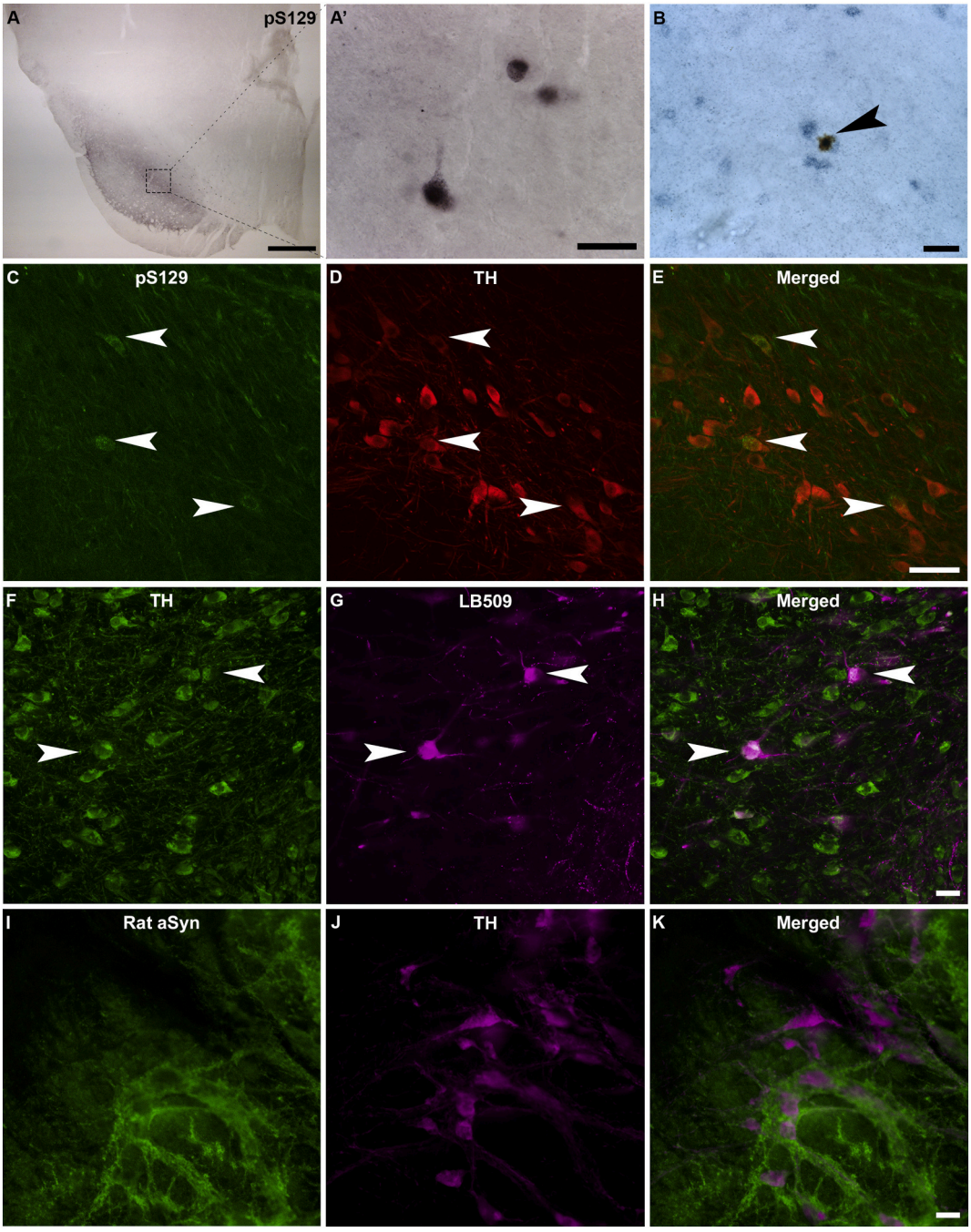

Fig. 3. Transfer of aSyn from oligodendrocytes to nigral neurons. Photomicrographs of the substantia nigra of HT Olig001-aSyn rats illustrates pS129+ aSyn immunoreactivity in neurons of the substantia nigra (a and a′). Scale bar: a = 500 μm, a′ = 25 μm. RNAscope in situ hybridization (b) of Olig001 AAV genome (brown) shows co-localization (arrowhead) with Olig2+ oligodendrocytes (blue) in the substantia nigra. Scale bar: 25 μm. Confocal microscopy illustrates immunoreactivity of pS129 (c) and TH (d) co-localization in nigral dopamine neurons (e). Scale bar: 50 μm. Co-localization (arrows) of TH (f) with human-specific LB509 aSyn (g) showing exogenous human origin of aSyn. Scale bar: 50 μm. Lack of co-localization of rodent-specific aSyn (i) with TH (j). Scale bar: 50 μm. (For interpretation of the references to colour in this figure legend, the reader is referred to the web version of this article.)

5.5. aSyn overexpression causes myelin loss and neurodegeneration in NHPs

We next examined the neuronal and axonal integrity seen in Olig-001 injected monkeys. In Olig001-aSyn NHPs, LB509+ aSyn staining in the CC (Fig. 5a) and putamen (Fig. 5c) corresponded to areas of decreased LFB staining observed in the CC (Fig. 5b) and white matter bundles throughout the putamen (Fig. 5d). Conversely, in regions of GFP expression (Fig. 5e and g), no changes in myelin were observed (Fig. 5f and h) in any NHP injected with the Olig001-GFP control vector.

As with rats, NeuN was used as a neuronal marker to evaluate the presence of degenerating neurons in the putamen of Olig001-injected monkeys. Stereological estimates revealed a decreased density and staining intensity of NeuN immunoreactivity throughout the entire putamen of Olig001-aSyn monkeys (Fig. 5j), whereas Olig001-GFP NHPs displayed a loss of NeuN+ staining only within in the immediate periphery of the site of injection (Fig. 5n). Unbiased stereological cell counts throughout the rostral-caudal extent of the putamen revealed a 43.4% loss of NeuN+ putamenal neurons in Olig001-aSyn injected monkeys when compared to Olig001-GFP controls (Fig. 5q, Olig001-

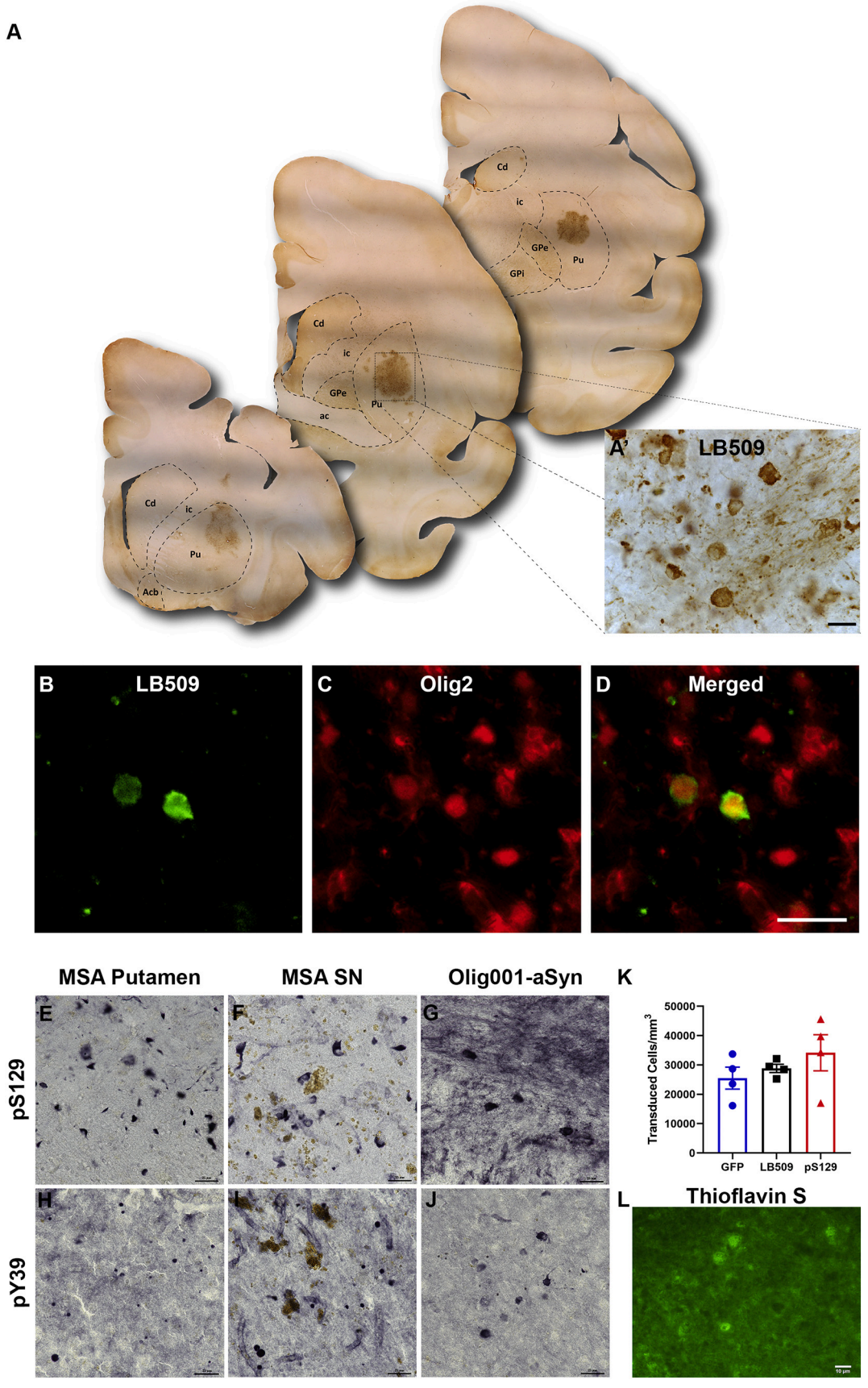

(caption on next page)

Fig. 4. Olig001 transduction and GCI formation in post-mortem MSA and Olig001 nonhuman primate brains. Photomicrographs of LB509 aSyn immunoreactivity throughout the rostro-caudal putamen of Olig001-aSyn injected NHPs (A). High magnification inset illustrating LB509+ GCIs (A′). Scale bar: A′ = 25 μm. LB509+ aSyn staining (b and d, green) surrounding the nuclear oligodendroglial Olig2+ signal (c and d, red) confirms the cytoplasmic location of the aSyn aggregates in NHP oligodendrocytes. Scale bar: b-d = 20 μm. Photomicrographs of post-translational modifications of aSyn shown by pS129 and pY39 aSyn immunoreactivity in post-mortem MSA putamen (E and H), substantia nigra (F and I), and Olig001-aSyn injected NHPs (G and J). Scale bars: *E*-J = 25 μm. Stereological analysis of the area of transduction in the putamen (K) revealed no significant difference in inclusions formed in Olig001 injected NHPs. Thioflavin S+ inclusions formed in Olig001-aSyn injected NHPs (L). Scale bar: L = 10 μm. Acb = nucleus accumbens, ac = anterior commissure, Cd = caudate, GPe = globus pallidus externus, GPi = globus pallidus interus, ic = internal capsule, Pu = putamen. N = 4/group. (For interpretation of the references to colour in this figure legend, the reader is referred to the web version of this article.)

aSyn: 26,177 ± 2050 NeuN+ cells/mm^3, Olig001-GFP: 46,267 ± 411.9 NeuN+ cells/mm^3, *$P \leq 0.05$). Using TH as a marker for nigral dopamine neurons, a loss of TH+ fibers and neurons were observed in the substantia nigra of Olig001-aSyn NHPs (Fig. 5k–l) compared to Olig001-GFP controls (Fig. 5o–p). Unbiased stereological cell counts throughout the rostral-caudal extent of the substantia nigra revealed an 11% loss of TH+ neurons in Olig001-aSyn injected monkeys when compared to Olig001-GFP controls (Fig. 5r, Olig001-aSyn: 4692 ± 118.1 TH+ cells/mm^3, Olig001-GFP: 5260 ± 202.9 TH+ cells/mm^3, *$P \leq 0.05$). Taken together, these results indicate that sustained overexpression of oligodendroglial aSyn in NHPs is able to elicit striatonigral degeneration that is observed in the pathogenesis of MSA-P.

5.6. Neuroinflammation associated with Oligodendroglial aSyn overexpression

The presence of neuroinflammation has been well established in synucleinopathies and recent work continues to highlight the immune system as a key driver of disease progression. In MSA, microgliosis and astrogliosis are prevalent pathologies observed post-mortem in primary sites of aSyn+ GCIs (Ishizawa et al., 2004; Refolo et al., 2018; Williams et al., 2020). HLA-DR (LN3), a MHC class II cell surface receptor, is a commonly used marker that is upregulated on microglia during activation. Microglial activation shown by increased HLA-DR immunoreactivity was observed to coincide with areas of aSyn expression throughout the entire putamen of Olig001-aSyn NHPs (Fig. 6a, a′, and c), while HLA-DR immunoreactivity seemed to be restricted to the specific injection site and needle tract in Olig001-GFP injected NHPs (Fig. 6b and d). Densitometric measurements revealed a statistically significant increase in HLA-DR staining in Olig001-aSyn injected monkeys compared to Olig001-GFP injected controls, indicating a greater prevalence of activated microglia due to the overexpression of aSyn in oligodendroglia (Fig. 6i, Olig001-aSyn: 18.54 ± 0.692 AFU, Olig001-GFP: 12.03 ± 1.032 AFU, *$P \leq 0.05$). The HLA-DR+ cells in Olig001-aSyn NHPs displayed morphological features typical of activated microglia, featuring large cell bodies with short, thick processes (Fig. 6c). Similar to the observed increased activation of microglia, Olig001-aSyn injected monkeys were found to display prominent astrogliosis in the putamen where aSyn+ GCIs were formed (Fig. 6e and e′), which was not observed in Olig001-GFP NHPs (Fig. 6f and f′). A significant increase in GFAP+ staining intensity was observed in Olig001-aSyn injected monkeys compared to Olig001-GFP injected controls (Fig. 6j, Olig001-aSyn: 16.5 ± 2.045 AFU, Olig001-GFP: 10.84 ± 1.110 AFU, *P ≤ 0.05). Recently, our group has shown that in addition to increased activation of microglia and astroglia, there is a significant infiltration of T cells into the CNS of post-mortem MSA samples in brain regions containing aSyn-rich GCIs that drives disease progression (Williams et al., 2020). Histological analysis confirmed a robust infiltration of CD3+ T cells in the putamen of Olig001-aSyn injected NHPs (Fig. 6g and g′), where minimal CD3+ cells were observed with GFP injection (Fig. 6h and h′). Unbiased stereological counts of CD3+ T cells indicate a 470% increase in Olig001-aSyn NHPs compared to Olig001-GFP controls (Fig. 6k, Olig001-aSyn: 17,543 ± 1017 CD3+ cells/mm^3, Olig001-GFP: 3076 ± 696 CD3+ cells/mm^3, *P ≤ 0.05). These results indicate that viral vector-mediated overexpression of aSyn in oligodendrocytes of NHPs causes reactive, neuroinflammaory phenotypes that mimic both the innate and adaptive immune responses observed in clinical MSA.

6. Discussion

Previous work by our group utilizing the novel oligotropic AAV Olig001 to model MSA resulted in 95% efficiency to specifically transduce striatal oligodendroglia in both rats and NHPs. Short term (3-month) overexpression of aSyn in NHPs produced the formation of insoluble, pS129+ GCIs throughout the caudate and putamen, causing demyelination and microglial activation in regions of aSyn overexpression. Critically, no evidence of neuronal loss was observed at this short time point (Mandel et al., 2017). The objective of the present study was to build upon our previous work and to characterize the neuropathology following long term viral vector-mediated overexpression of aSyn in rats and NHPs. Here we show viral titer-dependent formation of MSA-like pathology in rats indicating that a ~ 10-fold higher titer of Olig001-aSyn is required to elicit myelin disruption and neuronal loss, and that high titers do not lead to off-target transduction. Six months following Olig001-aSyn injection in NHPs, hyperphosphorylated, thioflavin S+ GCIs were formed throughout the rostrocaudal extent of the putamen, which elicited demyelination, astrogliosis, microglial activation, infiltration of T cells into the CNS, and neuronal loss in both the putamen and substantia nigra. The comprehensive array of neuropathological features observed in this model following Olig001-aSyn transduction faithfully recapitulate an MSA-P-like phenotype in both rats and nonhuman primates (Table 1). Many non-motor and features of dysautonomia, such as heart rate variability, impaired respiratory control, bladder dysfunction, and REM sleep behavior disorder, have been observed in the PLP-aSyn mouse, however these aspects of MSA were not addressed in the present study (Boudes et al., 2013Boudes et al., 2013; Fernagut et al., 2014; Flabeau et al., 2014; Kuzdas et al., 2013; Stefanova et al., 2005; Stemberger et al., 2010). Additionally, the failure to observe neuronal loss in our previous short –term (3 month) studies, and the presence of striatal and nigral loss in the present longer term (6 month) experiments, provides a temporal framework for which progressive neuronal loss between these two time points can be used for therapeutic interventions.

The Olig001-aSyn viral vector overexpression model of MSA, like transgenic mouse models of MSA, is based on the specific overexpression of human aSyn in oligodendroglia (Bassil et al., 2017; Kahle et al., 2002; Shults et al., 2005; Tanji et al., 2019; Yazawa et al., 2005). These similar strategies originated around the 1989 discovery of GCIs in patients with striatonigral degeneration, olivopontocerebellar atrophy, and Shy-Drager syndrome, uniting these three syndromes under the common disease MSA (Papp et al., 1989; Quinn, 1989). Filamentous aSyn was later identified as a major component of GCIs (Spillantini et al., 1998) and the notion that GCIs are central to the pathogenesis of MSA arose as the distribution of GCIs strongly correlated with the degree neuronal loss (Ozawa et al., 2004; Papp and Lantos, 1994). Post-mortem and experimental studies have shown that the aSyn present in GCIs has undergone a number of post-translational modifications, such as phosphorylation and nitration of tyrosine, and serine phosphorylation (Beyer, 2006; Beyer and Ariza, 2007; Duda et al., 2000a; Duda et al., 2000b; Fujiwara et al., 2002; Giasson et al., 2000; Kahle et al., 2002). In the present study, we have demonstrated that the aSyn present in the GCIs of Olig001-aSyn injected rats and monkeys has undergone post-

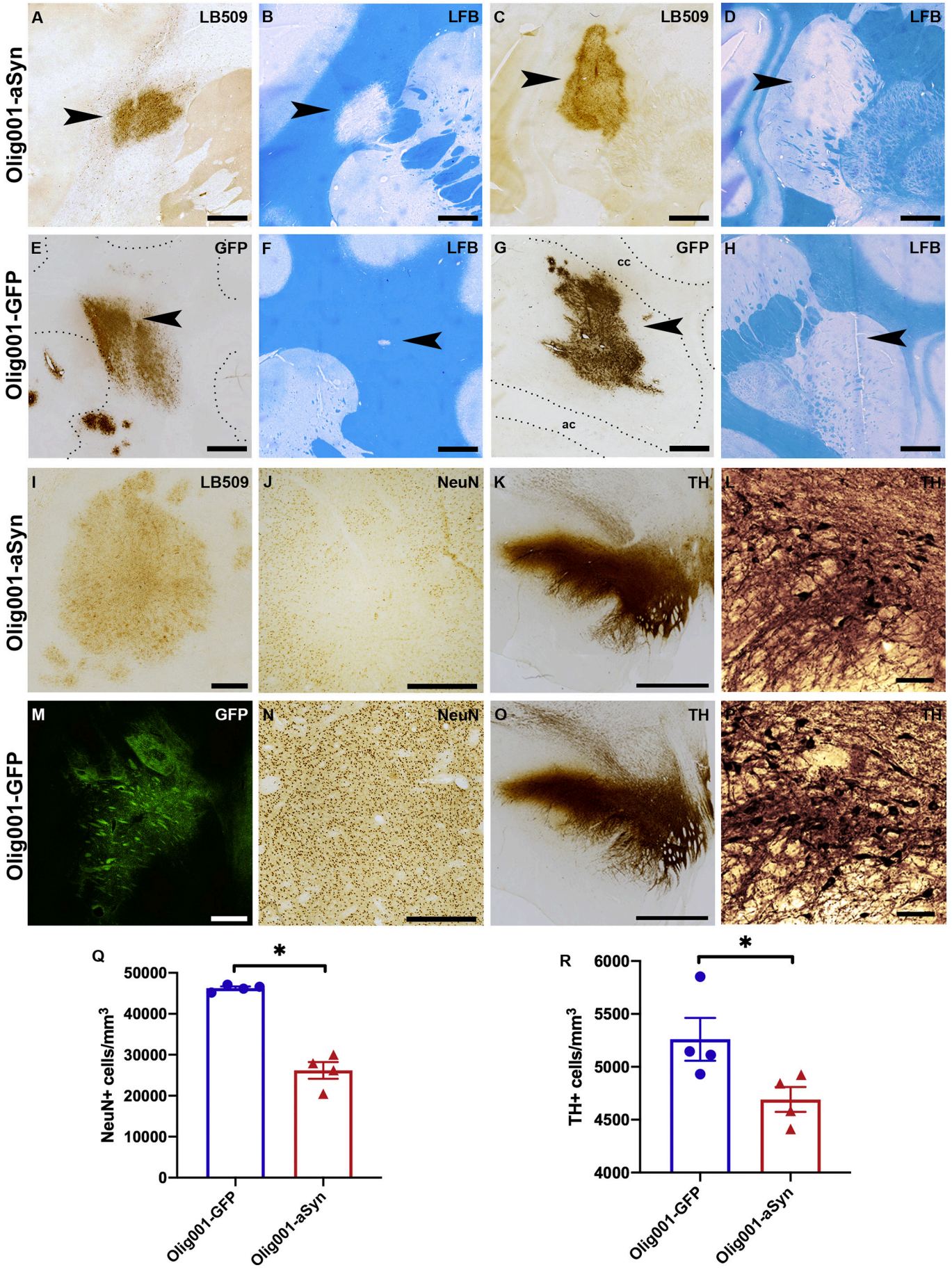

(caption on next page)

Fig. 5. Olig001-aSyn induced neurodegeneration in nonhuman primates. Photomicrograph of LB509 aSyn immunoreactivity in Olig001-aSyn injected NHPs (A and C) correspond to regions of demyelination in the corpus callosum and putamen (B and D respectively, arrowheads) in level matched sections shown by loss of LFB staining. GFP expression in Olig001-GFP NHPs (E and G) does not induce demyelination (f and h). Scale bars: A-H = 2000 μm. Photomicrograph of LB509+ aSyn staining (I) which correspond to decreased NeuN immunoreactivity in the putamen of Olig001-aSyn injected NHPs (J), whereas GFP expression (M) does not result in diminished NeuN immunoreactivity in Olig001-GFP NHPs (N). Scale bars: I and M = 1000 μm; J and *N* = 500 μm. Diminished TH+ fiber and neuronal staining in the substantia nigra of Olig001-aSyn NHPs (*K*,*L*) compared to Olig001-GFP NHPs (O, P). Scale bar K and O = 2000 μm, L and *P* = 100 μm. Stereological analysis revealed a significant loss of NeuN+ neurons in the putamen (Q, *P ≤ 0.05, Two-tailed Mann Whitney test) and TH+ neurons in the substantia nigra (R, *P ≤ 0.05, Two-tailed Mann Whitney test) of Olig001-aSyn NHPs compared to Olig001-GFP NHPs. N = 4/group.

translational modifications, as demonstrated by the abundant pS129 and pY39 immunoreactivity. Additionally, resistance to proteinase K digestion and thioflavin S staining indicates the formation of insoluble aggregates that have formed beta-pleated sheets as seen in authentic GCI's. Abnormal accumulation of fibrillary αSyn has also been reported in neuronal cytoplasm (NCIs) and nuclei (NNIs) as well as in neurites in post-mortem human MSA brains and in Olig001-aSyn injected animals (Papp and Lantos, 1994; Yoshida, 2007). NCIs are widely distributed throughout the brain, however unlike GCIs, their frequency does not seem to relate to the degree of neuron loss, highlighting the particular importance of GCIs to disease progression (Ozawa et al., 2004).

Despite the disruption of myelin observed in regions of GCI formation, the presence of aSyn inclusions in oligodendroglia is believed to disrupt the normal function of oligodendrocytes, but not oligodendroglial degeneration, as only minor changes to oligodendrocyte numbers have been reported in post-mortem MSA cases (Ettle et al., 2016; Nykjaer et al., 2017; Salvesen et al., 2015; Salvesen et al., 2017). In line with this concept, overt loss of oligodendroglia was not seen following aSyn overexpression using Olig001 in either rats or NHPs, while oligodendrocyte dysfunction was evident with respect to myelin integrity as observed by LFB staining and EM in areas of induced aSyn expression.

Another important oligodendroglial pathology during MSA pathogenesis is the accumulation of p25α/tubulin polymerization-promoting protein (TPPP) in GCIs in oligodendrocytes from patients with MSA (Kovács et al., 2004; Orosz et al., 2004; Takahashi et al., 1991). Under physiological conditions, p25α is localized in the myelin sheath and is functionally involved in the stabilization of microtubules and myelination, while relocation of p25α from the myelin sheath to the cytoplasm of oligodendroglia has been observed in MSA patients (Ovadi and Orosz, 2009; Song et al., 2007). This relocation correlates with a dramatic decrease of total MBP and an increase of degraded MBP (Kragh et al., 2009). Using antibodies directed towards p25α, the co-localization of p25α with LB509+ inclusions was seen in oligodendrocytes 1-month following injections of the highest titer of Olig001-aSyn in rats, which temporally corresponded with demyelination. Highlighting the relevance of p25α relocation and aSyn accumulation in GCIs, it has recently been shown that the overexpression of either p25α or aSyn in oligodendrocytes can enhance the recruitment of endogenous aSyn to form insoluble inclusions (Mavroeidi et al., 2019).

Despite the known link between aSyn, GCIs, and the progression of pathogenesis in MSA, the source of aSyn and the mechanism by which it accumulates in oligodendroglia remains heavily debated. In healthy brains, aSyn is found in nerve terminals and is believed to play an important role in synaptic transmission (Burre et al., 2014; Emamzadeh, 2016). Following the prion hypothesis of PD, one school of thought suggests aggregated aSyn can act as a prion that propagates throughout the neuraxis in MSA (Peng et al., 2018; Prusiner et al., 2015; Watts et al., 2013; Woerman et al., 2018). Experimentally, in vitro (Reyes et al., 2014) and in vivo (Rockenstein et al., 2012; Kaji et al., 2018) studies have shown that aSyn is able to transfer from neurons to oligodendrocytes. However, none of these studies have been able to replicate the formation of GCIs in wildtype animals (Dhillon et al., 2019). Another belief is that MSA is a primary oligodendrogliopathy with secondary neurodegeneration (Jellinger, 2015; Wenning et al., 2008). Conflicting studies exist showing the absence (Jin et al., 2008; Miller et al., 2005; Ozawa et al., 2001) or presence (Asi et al., 2014) of aSyn mRNA in oligodendroglia. Developmental studies using embryonic stem cells and induced pluripotent stem cells have shown the presence of aSyn protein and mRNA in oligodendrocyte precursor cells (OPCs) that diminishes upon cellular maturation (Djelloul et al., 2020), and that sustained expression of aSyn in OPCs hinders development of oligodendroglia and their ability to myelinate (Ettle et al., 2014; May et al., 2014). The notion that continuous expression of aSyn hinders oligodendrocyte development and function may raise questions as to the mechanism of neurodegeneration observed in tg MSA mice and its faithfulness to model the pathological progression of clinical MSA, as overexpression is continuous since birth in these models (Kahle et al., 2002; Shults et al., 2005; Yazawa et al., 2005). Viral vector-mediated overexpression (Bassil et al., 2017; Mandel et al., 2017) as well as inducible aSyn expression (Tanji et al., 2019) may get around this potential pitfall by overexpressing aSyn in adult animals, although viral vector-mediated induction avoids potential recombinant "leakiness" of Cre transgenic models. It will be important to further characterize the dynamics of synuclein aggregation within oligodendrocytes in this model, as putative synuclein "strains" derived from MSA patients have been suggested to produce a more toxic and aggregate-prone proteoforms (Strohäker et al., 2019; Yamasaki et al., 2019).

A growing body of work has highlighted the importance of the immune system playing a role in neurodegenerative diseases and synucleinopathies in particular. The aSyn-containing Lewy bodies and Lewy neurites in PD have been associated with increased HLA-DR+ microglia, and CD4+ and CD8+ T lymphocytes have been observed surrounding neuromelanin-laden nigral neurons, providing evidence for a aSyn-driven neuroinflammatory response (Allen Reish and Standaert, 2015; Brochard et al., 2009; Caggiu et al., 2019). Circulating T cells in the blood of PD patients have recently been shown to recognize aSyn peptides and produce increased release of pro-inflammatory cytokines compared to healthy controls (Sulzer et al., 2017). Studies in post-mortem MSA tissue and animal models of MSA have provided evidence of increased pro-inflammatory cytokines in the CSF and brain parenchyma, as well as microgliosis and astrogliosis in brain regions affected by the disease (Compta et al., 2019; La Holton and Revesez, 2013; Li et al., 2018; Refolo et al., 2018; Rydbirk et al., 2017; Stefanova et al., 2007; Stefanova et al., 2012; Yamasaki et al., 2017). The robust activation of microglia and astrogliosis observed in the current study, as shown by increased HLA-DR+ and GFAP+ staining in the putamen of Olig001-aSyn injected monkeys, parallels the growing body of evidence pointing towards an inflammatory response in MSA driven by aSyn and supports this model as faithfully reproducing this important feature of the human disease. Moreover, recent work by our group and others has shown robust infiltration of T lymphocytes into the brain parenchyma of MSA patients compared to controls (Rydbirk et al., 2017; Williams et al., 2020), which is recapitulated in the present study by showing a significant increase in the number of CD3+ T-cells in the putamen of Olig001 NHPs specific to aSyn.

It has been proposed that accumulation of aSyn in oligodendroglia leads to disruption of normal function, such as maintenance of myelin and neurotrophic support, resulting in secondary neuronal degeneration. As previously mentioned, accumulating aSyn causes glial activation, T cell infiltration, and release of pro-inflammatory cytokines, all of which contribute to neurodegeneration observed in MSA. Our previous work using Olig001 resulted in the formation of early stage neuropathology observed in MSA (Mandel et al., 2017). By sacrificing at later

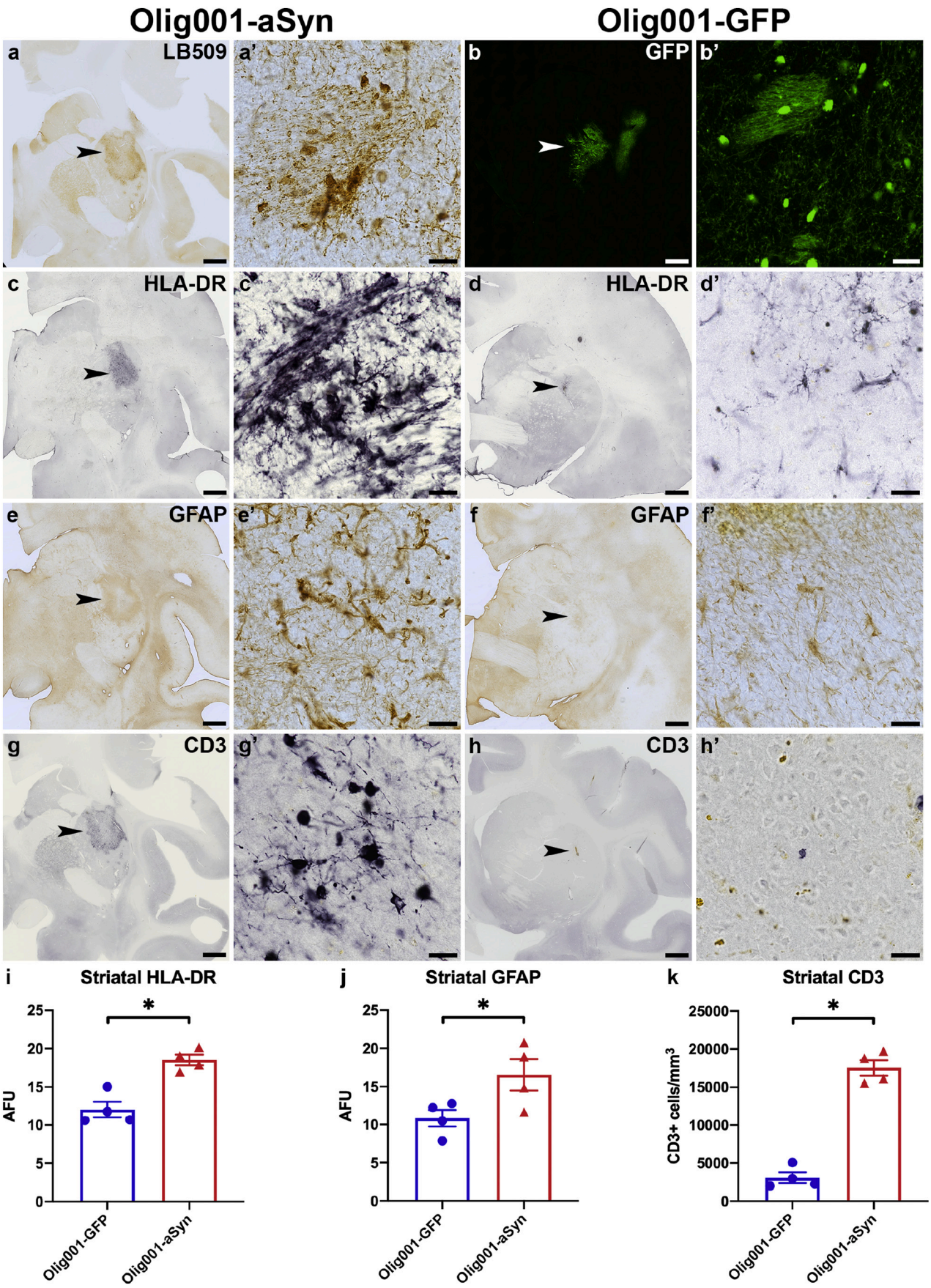

(caption on next page)

Fig. 6. Olig001-aSyn induced neuroinflammation in nonhuman primates. Photomicrographs showing transgene expression (A-B′), and associated microgliosis illustrated by HLA-DR immunoreactivity (C-D'), astrogliosis shown by GFAP immunoreactivity (E-F′), and T-cell response shown by CD3 immunoreactivity (G-H′) in level matched sections of Olig001-aSyn and Olig001-GFP NHPs. Arrowheads denote transduction area and region of high magnification image. Scale bars: A-H = 2000 μm; A′–H′ = 25 μm. Optical density measurements of HLA-DR stained tissue (I) revealed a significant increase of microglial activation in Olig001-aSyn NHPs compared to Olig001-GFP NHPs *P ≤ 0.05, Two-tailed Mann Whitney test). Optical density measurements of GFAP stained tissue (J) revealed a significant increase of astrogliosis in Olig001-aSyn NHPs compared to Olig001-GFP NHPs *P ≤ 0.05). Stereological analysis of CD3+ cells (K) revealed a significant increase in T-cell infiltration in the putamen of Olig001-aSyn NHPs compared to Olig001-GFP NHPs *P ≤ 0.05, Two-tailed Mann Whitney test). N = 4/group.

time points and increasing the volume of Olig001, we were able to induce neuronal loss in both the putamen and substantia nigra in the present study. Using activity monitors and the hand reach test to assess overall behavioral changes and fine motor dysfunction in monkeys, we did not observe any significant motor deficits in the present study (Supplementary Fig. 3). Given that we only observed an ~12% loss of nigral dopaminergic neurons in these monkeys, it is understandable that a behavioral deficit was not seen at this time, as the threshold for the appearance of motor symptoms was shown to require an ~80% loss of striatal dopamine content and ~43% nigral dopaminergic neuron degeneration experimentally in MPTP-lesioned NHPs and in post-mortem PD cases (Bezard et al., 2001; Kordower et al., 2013). TH cell loss was less than wat is typically seen in MSA-P, but future studies will utilize larger doses of Olig001 vector, which will a greater amount of neuronal loss, thus producing an observable motor deficit.

Unfortunately, there are currently no available potent symptomatic or disease modifying therapies for MSA and symptomatic therapies have not drastically changed over the last decade (Krismer and Wenning, 2017; Lopez-Cuina et al., 2018). Dysautonomia can be managed with drugs marketed to treat orthostatic hypotension and urinary dysfunction and antiparkinsonian dopaminergic medications may work on a subset of MSA-P patients (Perez-Lloret et al., 2015). Using proper animal models in pre-clinical testing of experimental therapeutics is a necessity for adequate translation into clinical trials. Studying neurological disorders in NHPs provides advantages over the use of rodents. Anatomically, the striatum in rodents is a single entity pierced by cortical white matter fibers, whereas in humans and NHPs, the striatal mass is separated into the caudate nucleus and putamen by the internal capsule. It is known that white matter tracts affect the distribution of intracerebrally injected compounds, thus studies involving striatal injections may offer more accurate translation into humans when modeled in NHPs (Marmion and Kordower, 2018). Furthermore, the size and organization of the NHP brain, as well as the glia-to-neuron ratio, is much more similar to humans than that of a mouse brain, which is important when studying glial diseases and in therapies that will attempt to clear or prevent the formation of GCIs in a larger brain. The Olig001 NHP model of MSA has several neuropathological features, such as myelination, neuroinflammation, GCI formation, and neuronal counts, which can be used as outcome measures in pre-clinical studies testing the efficacy of disease modifying therapies of MSA.

Supplementary data to this article can be found online at https://doi.org/10.1016/j.nbd.2020.105184.

Table 1
Comparison of pathological features observed in the Olig001 NHP model of MSA and clinical MSA in humans.

	Olig001-aSyn NHP (3 month)	Olig001-aSyn NHP (6 Month)	Human MSA
GCIs	Yes	Yes	Yes
PK Resistant aSyn	Yes	Yes	Yes
Thioflavin S+ Inclusions	N/A	Yes	Yes
pS129+ aSyn	Yes	Yes	Yes
pY39+ aSyn	N/A	Yes	Yes
p25α Relocation	N/A	Yes	Yes
Demyelination	Yes	Yes	Yes
Neuronal Loss	No	Yes; Striatum & Substantia Nigra	Yes
Microglial Activation	Yes	Yes	Yes
Astrogliosis	N/A	Yes	Yes
T-Cells in CNS	Yes	Yes	Yes
Oligodendroglial Loss	No	No	No
Motor Symptoms	No	No	Yes
Autonomic Dysfunction	N/A	N/A	Yes

N/A: Not assessed, GCIs: Glial Cytoplasmic Inclusions, PK: proteinase K, pS129: phosphorylated serine at residue 129, pY39: phosphorylated tyrosine at residue 39.

Author contributions

DJM participated in the design, rodent and nonhuman primate surgeries, collecting data, data analysis, and writing the manuscript. AAR, BMH and DC participated in collecting the data. MHW, EB, and DK participated in the design, data analysis, and writing the manuscript. TM and SJG developed and produced the Olig001 vector. JHK participated in the design, nonhuman primate surgery, data analysis, and writing the manuscript.

Ethical approval and consent to participate

Ethical approval for the collection and use of post-mortem brain tissue used in this study was obtained from the Rush University Medical Center IRB.

Ethical approval for the use of animals and all procedures were approved by the University of Illinois Chicago Institutional Animal Care and Use Committee and the Rush University Institutional Animal Care and Use Committee and accredited by the Association for Assessment and Accreditation of Laboratory Animal Care. Animals were cared for in accordance with the principles of the Guide to the Care and Use of Experimental Animals. Animal care was supervised by veterinarians skilled in the care and maintenance of non-human primates.

Consent for publication

Not applicable.

Funding

This work was supported by a grant to JHK from the MSA Coalition.

Declaration of Competing Interest

Drs. Gray and McCown are inventors on a patent for the Olig001 capsid, and have received royalty income from Asklepios Biopharma related to this invention.

Acknowledgements

We would like to acknowledge Scott Muller and Rachel Harker for their assistance with nonhuman primate surgery and behavior and Dr. Poul Henning Jensen for his generous donation of p25α antibody.

References

Allen Reish, H.E., Standaert, D.G., 2015. Role of alpha-synuclein in inducing innate and adaptive immunity in Parkinson disease. J. Parkinsons Dis. 5 (1), 1–19. https://doi.org/10.3233/JPD-140491.

Alvarez, A.R., Klein, A., Castro, J., Cancino, G.I., Amigo, J., Mosqueira, M., et al., 2008. Imatinib therapy blocks cerebellar apoptosis and improves neurological symptoms in a mouse model of Niemann-pick type C disease. FASEB J. 22 (10), 3617–3627. https://doi.org/10.1096/fj.07-102715 (Epub 2008 Jun 30).

Asi, Y.T., Simpson, J.E., Heath, P.R., Wharton, S.B., Lees, A.J., Revesz, T., et al., 2014. Alpha-synuclein mRNA expression in oligodendrocytes in MSA. Glia 62 (6), 964–970. https://doi.org/10.1002/glia.22653.

Bassil, F., Guerin, P.A., Dutheil, N., Li, Q., Klugmann, M., Meissner, W.G., et al., 2017. Viral-mediated oligodendroglial alpha-synuclein expression models multiple system atrophy. Mov. Disord. 32 (8), 1230–1239. https://doi.org/10.1002/mds.27041.

Beyer, K., 2006. Alpha-synuclein structure, posttranslational modification and alternative splicing as aggregation enhancers. Acta Neuropathol. 112, 237–251.

Beyer, K., Ariza, A., 2007. Protein aggregation mechanisms in synucleinopathies: commonalities and differences. J. Neuropathol. Exp. Neurol. 66, 965–974.

Bezard, E., Dovero, S., Prunier, C., Ravenscroft, P., Chalon, S., Guilloteau, D., et al., 2001. Relationship between the appearance of symptoms and the level of nigrostriatal degeneration in a progressive 1-methyl-4-phenyl-1,2,3,6-tetrahydropyridine-lesioned macaque model of Parkinson's disease. J. Neurosci. 21 (17), 6853–6861. https://doi.org/10.1523/JNEUROSCI.21-17-06853.2001.

Boudes, M., Uvin, P., Pinto, S., Voets, T., Fowler, C.J., Wenning, G.K., et al., 2013. Bladder dysfunction in a transgenic mouse model of multiple system atrophy. Mov. Disord. 28 (3), 347–355.

Bower, J.H., Maraganore, D.M., McDonnell, S.K., Rocca, W.A., 1997. Incidence of progressive supranuclear palsy and multiple system atrophy in Olmsted County, Minnesota, 1976 to 1990. Neurology 49, 1284–1288.

Brahmachari, S., Ge, P., Lee, S.H., Kim, D., Karuppagounder, S.S., Kumar, M., et al., 2016. Activation of tyrosine kinase c-Abl contributes to α-synuclein-induced neurodegeneration. J. Clin. Invest. 126 (8), 2970–2988. https://doi.org/10.1172/JCI85456.

Brahmachari, S., Lee, S., Kim, S., Yuan, C., Karuppagounder, S.S., Ge, P., et al., 2019. Parkin interacting substrate zinc finger protein 746 is a pathological mediator in Parkinson's disease. Brain. 142 (8), 2380–2401. https://doi.org/10.1093/brain/awz172.

Brochard, V., Combadiere, B., Prigent, A., Laouar, Y., Perrin, A., Beray-Berthat, V., et al., 2009. Infiltration of CD4+ lymphocytes into the brain contributes to neurodegeneration in a mouse model of Parkinson disease. J. Clin. Invest. 119 (1), 182–192. https://doi.org/10.1172/JCI36470.

Burre, J., Sharma, M., Sudhof, T.C., 2014. α-Synuclein assembles into higher-order multimers upon membrane binding to promote SNARE complex formation. Proc. Natl. Acad. Sci. U. S. A. 111 (40), E4274–E4283. https://doi.org/10.1073/pnas.1416598111.

Caggiu, E., Arru, G., Hosseini, S., Niegowska, M., Sechi, G., Zarbo, I.R., et al., 2019. Inflammation, infectious triggers, and Parkinson's disease. Front. Neurol. 10, 122. https://doi.org/10.3389/fneur.2019.00122.

Cancino, G.I., Toledo, E.M., Leal, N.R., Hernandez, D.E., Yévenes, L.F., Inestrosa, N.C., et al., 2008. STI571 prevents apoptosis, tau phosphorylation and behavioural impairments induced by Alzheimer's beta-amyloid deposits. Brain. 131 (Pt 9), 2425–2442. https://doi.org/10.1093/brain/awn125 (Epub 2008 Jun 17).

Chu, Y., Le, W., Kompoliti, K., Jankovic, J., Mufson, E.J., Kordower, J.H., 2006. Nurr1 in Parkinson's disease and related disorders. J. Comp. Neurol. 494, 495–514.

Compta, Y., Dias, S.P., Giraldo, D.M., Perez-Soriano, A., Munoz, E., Saura, J., et al., 2019. Cerebrospinal fluid cytokines in multiple system atrophy: a cross-sectional Catalan MSA registry study. Parkinsonism Relat. Disord. 65, 3–12. https://doi.org/10.1016/j.parkreldis.2019.05.040.

Dhillon, J.S., Trejo-Lopez, J.A., Riffe, C., Levites, Y., Sacino, A.N., Borchelt, D.R., et al., 2019. Comparative analyses of the in vivo induction and transmission of α-synuclein pathology in transgenic mice by MSA brain lysate and recombinant α-synuclein fibrils. Acta Neuropathol. Commun. 7 (1), 80. https://doi.org/10.1186/s40478-019-0733-3.

Djelloul, M., Holmqvist, S., Boza-Serrano, A., Azevedo, C., Yeung, M.S., Goldwurm, S., et al., 2020. Alpha-synuclein expression in the oligodendrocyte lineage: an in vitro and in vivo study using rodent and human models. Stem Cell Rep. 5 (2), 174–184. https://doi.org/10.1016/j.stemcr.2015.07.002.

Duda, J.E., Giasson, B.I., Chen, Q., Gur, T.L., Hurtig, H.I., Stern, M.B., Gollomp, S.M., Ischiropoulos, H., Lee, V.M., Trojanowski, J.Q., 2000a. Widespread nitration of pathological inclusions in neurodegenerative synucleinopathies. Am. J. Pathol. 157, 1439–1445.

Duda, J.E., Giasson, B.I., Gur, T.L., Montine, T.J., Robertson, D., Biaggioni, I., Hurtig, H. I., Stern, M.B., Gollomp, S.M., Grossman, M., Lee, V.M., Trojanowski, J.Q., 2000b. Immunohistochemical and biochemical studies demonstrate a distinct profile of alpha-synuclein permutations in multiple system atrophy. J. Neuropathol. Exp. Neurol. 59, 830–841.

Emamzadeh, F.N., 2016. Alpha-synuclein structure, functions, and interactions. J. Res. Med. Sci. 21, 29. https://doi.org/10.4103/1735-1995.181989.

Emborg, M.E., Ma, S.Y., Mufson, E.J., Levey, A.I., Taylor, M.D., Brown, W.D., et al., 1998. Age-related declines in nigral neuronal function correlate with motor impairments in rhesus monkeys. J. Comp. Neurol. 401 (2), 253–265.

Ettle, B., Reiprich, S., Deusser, J., Schlachetzki, J.C., Xiang, W., Prots, I., et al., 2014. Intracellular alpha-synuclein affects early maturation of primary oligodendrocyte progenitor cells. Mol. Cell. Neurosci. 62, 68–78. https://doi.org/10.1016/j.mcn.2014.06.012.

Ettle, B., Schlachetzki, J.C., Winkler, J., 2016. Oligodendroglia and myelin in neurodegenerative diseases: more than just bystanders? Mol. Neurobiol. 53 (5), 3046–3062. https://doi.org/10.1007/s12035-015-9205-3.

Fernagut, P.O., Meissner, W.G., Biran, M., Fantin, M., Bassil, F., Franconi, J.M., et al., 2014. Age-related motor dysfunction and neuropathology in a transgenic mouse model of multiple system atrophy. Synapse 68 (3), 98–106. https://doi.org/10.1002/syn.21719.

Flabeau, O., Meissner, W.G., Ozier, A., Berger, P., Tison, F., Fernagut, P.O., 2014. Breathing variability and brainstem serotonergic loss in a genetic model of multiple system atrophy. Mov. Disord. 29 (3), 388–395.

Fujiwara, H., Hasegawa, M., Dohmae, N., Kawashima, A., Masliah, E., Goldberg, M.S., et al., 2002. α-Synuclein is phosphorylated in synucleinopathy lesions. Nat. Cell Biol. 4, 160–164.

Giasson, B.I., Duda, J.E., Murray, I.V., Chen, Q., Souza, J.M., Hurtig, H.I., Ischiropoulos, H., Trojanowski, J.Q., Lee, V.M., 2000. Oxidative damage linked to neurodegeneration by selective alpha-synuclein nitration in synucleinopathy lesions. Science 290, 985–989.

Gilman, S., Wenning, G.K., Low, P.A., Brooks, D.J., Mathias, C.J., Trojanowski, J.Q., et al., 2008. Second consensus statement on the diagnosis of multiple system atrophy. Neurology. 71 (9), 670–676. https://doi.org/10.1212/01.wnl.0000324625.00404.15.

Grabinski, T.M., Kneynsberg, A., Manfredsson, F.P., Kanaan, N.M., 2015. A method for combining RNAscope in situ hybridization with immunohistochemistry in thick free-floating brain sections and primary neuronal cultures. PLoS One 10 (3), e0120120. https://doi.org/10.1371/journal.pone.0120120.

Gray, S.J., Foti, S.B., Schwartz, J.W., Bachaboina, L., Taylor-Blake, B., Coleman, J., et al., 2011. Optimizing promoters for recombinant adeno-associated virus-mediated gene expression in the peripheral and central nervous system using self-complementary vectors. Hum. Gene Ther. 22 (9), 1143–1153. https://doi.org/10.1089/hum.2010.245.

Hebron, M.L., Lonskaya, I., Moussa, C.E., 2013. Nilotinib reverses loss of dopamine neurons and improves motor behavior via autophagic degradation of α-synuclein in Parkinson's disease models. Hum. Mol. Genet. 22 (16), 3315–3328. https://doi.org/10.1093/hmg/ddt192.

Imam, S.Z., Zhou, Q., Yamamoto, A., Valente, A.J., Ali, S.F., Bains, M., et al., 2011. Novel regulation of parkin function through c-Abl-mediated tyrosine phosphorylation: implications for Parkinson's disease. J. Neurosci. 31 (1), 157–163. https://doi.org/10.1523/JNEUROSCI.1833-10.2011.

Ishizawa, K., Komori, T., Sasaki, S., Arai, N., Mizutani, T., Hirose, T., 2004. Microglial activation parallels system degeneration in multiple system atrophy. J. Neuropathol. Exp. Neurol. 63 (1), 43–52.

Jellinger, K.A., 2014. Neuropathology of multiple system atrophy: new thoughts about pathogenesis. Mov. Disord. 29 (14), 1720–1741. https://doi.org/10.1002/mds.26052.

Jellinger, K.A., 2015. Multiple system atrophy—a synucleinopathy with specific glioneuronal degeneration. Austin J. Clin. Neurol. 2015 (2), 1071.

Jellinger, K.A., Seppi, K., Wenning, G.K., 2005. Grading of neuropathology in multiple system atrophy: proposal for a novel scale. Mov. Disord. 20 (Suppl. 12), S29–S36.

Jin, H., Ishikawa, K., Tsunemi, T., Ishiguro, T., Amino, T., Mizusawa, H., 2008. Analyses of copy number and mRNA expression level of the alpha-synuclein gene in multiple system atrophy. J. Med. Dent. Sci. 55 (1), 145–153.

Jing, Z., Caltagarone, J., Bowser, R., 2009. Altered subcellular distribution of c-Abl in Alzheimer's disease. J. Alzheimers Dis. 17 (2), 409–422. https://doi.org/10.3233/JAD-2009-1062.

Kahle, P.J., Neumann, M., Ozmen, L., Muller, V., Jacobsen, H., Spooren, W., et al., 2002. Hyperphosphorylation and insolubility of alpha-synuclein in transgenic mouse oligodendrocytes. EMBO Rep. 3 (6), 583–588.

Kaji, S., Maki, T., Kinoshita, H., Uemura, N., Ayaki, T., Kawamoto, Y., et al., 2018. Pathological endogenous α-Synuclein accumulation in oligodendrocyte precursor cells potentially induces inclusions in multiple system atrophy. Stem Cell Rep. 10 (2), 356–365. https://doi.org/10.1016/j.stemcr.2017.12.001.

Ko, H.S., Lee, Y., Shin, J.H., Karuppagounder, S.S., Gadad, B.S., Koleske, A.J., et al., 2010. Phosphorylation by the c-Abl protein tyrosine kinase inhibits parkin's ubiquitination and protective function. Proc. Natl. Acad. Sci. U. S. A. 107 (38), 16691–16696. https://doi.org/10.1073/pnas.1006083107.

Kordower, J.H., Chu, Y., Hauser, R.A., Freeman, T.B., Olanow, C.W., 2008. Lewy body-like pathology in long-term embryonic nigral transplants in Parkinson's disease. Nat. Med. 14, 504–506.

Kordower, J.H., Olanow, C.W., Dodiya, H.B., Chu, Y., Beach, T.G., Adler, C.H., et al., 2013. Disease duration and the integrity of the nigrostriatal system in Parkinson's disease. Brain. 136 (Pt 8), 2419–2431. https://doi.org/10.1093/brain/awt192.

Kovács, G.G., László, L., Kovács, J., Jensen, P.H., Lindersson, E., Botond, G., et al., 2004. Natively unfolded tubulin polymerization promoting protein TPPP/p25 is a common marker of alpha-synucleinopathies. Neurobiol. Dis. 17, 155–162.

Kragh, C.L., Lund, L.B., Febbraro, F., Hansen, H.D., Gai, W.P., El-Agnaf, O., et al., 2009. Alpha-synuclein aggregation and Ser-129 phosphorylation-dependent cell death in oligodendroglial cells. J. Biol. Chem. 284 (15), 10211–10222. https://doi.org/10.1074/jbc.M809671200.

Krismer, F., Wenning, G.K., 2017. Multiple system atrophy: insights into a rare and debilitating movement disorder. Nat. Rev. Neurol. 13 (4), 232–243.

Kuzdas, D., Stemberger, S., Gaburro, S., Stefanova, N., Singewald, N., Wenning, G.K., 2013. Oligodendroglial alpha-synucleinopathy and MSA-like cardiovascular autonomic failure: experimental evidence. Exp. Neurol. 247, 531–536.

La Holton, J.L., Revesez, T., 2013. Multiple system atrophy in neurodegeneration. In: Dickson, D.W.W.R. (Ed.), The Molecular Pathology of Dementia and Movement Disorders, 2nd ed. Blackwell Publishing Ltd., Oxford, pp. 242–252.

Li, F., Ayaki, T., Maki, T., Sawamoto, N., Takahashi, R., 2018. NLRP3 inflammasome-related proteins are upregulated in the putamen of patients with multiple system atrophy. J. Neuropathol. Exp. Neurol. 77, 1055–1065. https://doi.org/10.1093/jnen/nly090.

Lopez-Cuina, M., Foubert-Samier, A., Tison, F., Meissner, W.G., 2018. Present and future of disease –modifying therapies in multiple system atrophy. Auton. Neurosci. 211, 31–38.

Low, P.A., Reich, S.G., Jankovic, J., Shults, C.W., Stern, M.B., Novak, P., et al., 2015. Natural history of multiple system atrophy in the USA: a prospective cohort study. Lancet Neurol. 14 (7), 710–719. https://doi.org/10.1016/S1474-4422(15)00058-7.

Mahul-Mellier, A.L., Fauvet, B., Gysbers, A., Dikiy, I., Oueslati, A., Georgeon, S., et al., 2014. C-Abl phosphorylates α-synuclein and regulates its degradation: implication for α-synuclein clearance and contribution to the pathogenesis of Parkinson's disease. Hum. Mol. Genet. 23 (11), 2858–2879. https://doi.org/10.1093/hmg/ddt674 (Epub 2014 Jan 9).

Mandel, R.J., Marmion, D.J., Kirik, D., Chu, Y., Heindel, C., McCown, T., et al., 2017. Novel oligodendroglial alpha synuclein viral vector models of multiple system atrophy: studies in rodents and nonhuman primates. Acta Neuropathol. Commun. 5 (1), 47. https://doi.org/10.1186/s40478-017-0451-7.

Marmion, D.J., Kordower, J.H., 2018. α-Synuclein nonhuman primate models of Parkinson's disease. J. Neural Transm. (Vienna) 125 (3), 385–400. https://doi.org/10.1007/s00702-017-1720-0.

Martí, M.J., Tolosa, E., Campdelacreu, J., 2003. Clinical overview of the synucleinopathies. Mov. Disord. 18 (Suppl. 6), S21–S27.

Mavroeidi, P., Arvanitaki, F., Karakitsou, A.K., Vetsi, M., Kloukina, I., Zweckstetter, M., et al., 2019. Endogenous oligodendroglial alpha-synuclein and TPPP/p25α orchestrate alpha-synuclein pathology in experimental multiple system atrophy models. Acta Neuropathol. 138 (3), 415–441. https://doi.org/10.1007/s00401-019-02014-y.

May, V.E., Ettle, B., Poehler, A.M., Nuber, S., Ubhi, K., Rockenstein, E., et al., 2014. α-Synuclein impairs oligodendrocyte progenitor maturation in multiple system atrophy. Neurobiol. Aging 35 (10), 2357–2368. https://doi.org/10.1016/j.neurobiolaging.2014.02.028.

Miller, D.W., Johnson, J.M., Solano, S.M., Hollingsworth, Z.R., Standaert, D.G., Young, A.B., 2005. Absence of alpha-synuclein mRNA expression in normal and multiple system atrophy oligodendroglia. J. Neural Transm. 112 (12), 1613–1624. https://doi.org/10.1007/s00702-005-0378-1.

Nykjaer, C.H., Brudek, T., Salvesen, L., Pakkenberg, B., 2017. Changes in the cell population in brain white matter in multiple system atrophy. Mov. Disord. 32 (7), 1074–1082.

Orosz, F., Kovacs, G.G., Lehotzky, A., Olah, J., Vincze, O., Ovadi, J., 2004. TPPP/p25: from unfolded protein to misfolding disease: prediction and experiments. Biol. Cell. 96, 701–711.

Ota, K., Obayashi, M., Ozaki, K., Ichinose, S., Kakita, A., Tada, M., et al., 2014. Relocation of p25α/tubulin polymerization promoting protein from the nucleus to the perinuclear cytoplasm in the oligodendroglia of sporadic and COQ2 mutant multiple system atrophy. Acta Neuropathol. Commun. 2, 136. https://doi.org/10.1186/s40478-014-0136-4.

Ovadi, J., Orosz, F., 2009. An unstructured protein with destructive potential: TPPP/p25 in neurodegeneration. Bioessays 31, 676–686.

Ozawa, T., Okuizumi, K., Ikeuchi, T., Wakabayashi, K., Takahashi, H., Tsuji, S., 2001. Analysis of the expression level of alpha-synuclein mRNA using postmortem brain samples from pathologically confirmed cases of multiple system atrophy. Acta Neuropathol. 102 (2), 188–190.

Ozawa, T., Paviour, D., Quinn, N.P., Josephs, K.A., Sangha, H., Kilford, L., et al., 2004. The spectrum of pathological involvement of the striatonigral and olivopontocerebellar systems in multiple system atrophy: clinicopathological correlations. Brain 127, 2657–2671.

Papapetropoulos, S., Tuchman, A., Laufer, D., Papatsoris, A.G., Papapetropoulos, N., Mash, D.C., 2007. Causes of death in multiple system atrophy. J. Neurol. Neurosurg. Psychiatry 78 (3), 327–329.

Papp, M.I., Lantos, P.L., 1994. The distribution of oligodendroglial inclusions in multiple system atrophy and its relevance to clinical symptomatology. Brain 117 (Pt 2), 235–243.

Papp, M.I., Kahn, J.E., Lantos, P.L., 1989. Glial cytoplasmic inclusions in the CNS of patients with multiple system atrophy (striatonigral degeneration, olivopontocerebellar atrophy and shy-Drager syndrome). J. Neurol. Sci. 94 (1–3), 79–100.

Peng, C., Gathagan, R.J., Covell, D.J., Medellin, C., Stieber, A., Robinson, J.L., et al., 2018. Cellular milieu imparts distinct pathological alpha-synuclein strains in alpha -synucleinopathies. Nature 557 (7706), 558–563.

Perez-Lloret, S., Flabeau, O., Fernagut, P.O., Pavy-Le Traon, A., Rey, M.V., Foubert-Samier, A., et al., 2015. Current concepts in the treatment of multiple system atrophy. Mov. Disord. Clin. Pract. 2 (1), 6–16.

Powell, S.K., Khan, N., Parker, C.L., Samulski, R.J., Matsushima, G., Gray, S.J., et al., 2016. Characterization of a novel adeno-associated viral vector with preferential oligodendrocyte tropism. Gene Ther. 23 (11), 807–814. https://doi.org/10.1038/gt.2016.62.

Prusiner, S.B., Woerman, A.L., Mordes, D.A., Watts, J.C., Rampersaud, R., Berry, D.B., et al., 2015. Evidence for alpha-synuclein prions causing multiple system atrophy in humans with parkinsonism. Proc. Natl. Acad. Sci. U. S. A. 112 (38), E5308–E5317.

Quinn, N., 1989. Multiple system atrophy–the nature of the beast. J. Neurol. Neurosurg. Psychiatry 78–89.

Refolo, V., Bez, F., Polissidis, A., Kuzdas-Wood, D., Sturm, E., Kamaratou, M., et al., 2018. Progressive striatonigral degeneration in a transgenic mouse model of multiple system atrophy: translational implications for interventional therapies. Acta Neuropathol. Commun. 6 (1), 2. https://doi.org/10.1186/s40478-017-0504-y.

Reyes, J.F., Rey, N.L., Bousset, L., Melki, R., Brundin, P., Angot, E., 2014. Alpha-synuclein transfers from neurons to oligodendrocytes. Glia 62 (3), 387–398. https://doi.org/10.1002/glia.22611.

Rockenstein, E., Ubhi, K., Inglis, C., Mante, M., Patrick, C., Adame, A., et al., 2012. Neuronal to oligodendroglial alpha-synuclein redistribution in a double transgenic model of multiple system atrophy. Neuroreport 23 (4), 259–264.

Rydbirk, R., Elfving, B., Andersen, M.D., Langbol, M.A., Folke, J., Winge, K., et al., 2017. Cytokine profiling in the prefrontal cortex of Parkinson's disease and multiple system atrophy patients. Neurobiol. Dis. 106, 269–278. https://doi.org/10.1016/j.nbd.2017.07.014.

Salvesen, L., Ullerup, B.H., Sunay, F.B., Brudek, T., Løkkegaard, A., Agander, T.K., et al., 2015. Changes in total cell numbers of the basal ganglia in patients with multiple system atrophy - a stereological study. Neurobiol. Dis. 74, 104–113. https://doi.org/10.1016/j.nbd.2014.11.008.

Salvesen, L., Winge, K., Brudek, T., Agander, T.K., Lokkegaard, A., Pakkenberg, B., 2017. Neocortical neuronal loss in patients with multiple system atrophy: a stereological study. Cereb. Cortex 27, 400–410.

Schlatterer, S.D., Acker, C.M., Davies, P., 2011. C-Abl in neurodegenerative disease. J. Mol. Neurosci. 45 (3), 445–452. https://doi.org/10.1007/s12031-011-9588-1.

Schrag, A., Wenning, G.K., Quinn, N., Ben-Shlomo, Y., 2008. Survival in multiple system atrophy. Mov. Disord. 23 (2), 294–296. https://doi.org/10.1002/mds.21839.

Schweighauser, M., Shi, Y., Tarutani, A., Kametani, F., Murzin, A.G., Ghetti, B., et al., 2020. Structures of α-synuclein filaments from multiple system atrophy. Nature. https://doi.org/10.1038/s41586-020-2317-6.

Shults, C.W., Rockenstein, E., Crews, L., Adame, A., Mante, M., Larrea, G., et al., 2005. Neurological and neurodegenerative alterations in a transgenic mouse model expressing human alpha-synuclein under oligodendrocyte promoter: implications for multiple system atrophy. J. Neurosci. 25, 10689–10699.

Song, Y.J., Lundvig, D.M., Huang, Y., Gai, W.P., Blumbergs, P.C., Hojrup, P., et al., 2007. p25alpha relocalizes in oligodendroglia from myelin to cytoplasmic inclusions in multiple system atrophy. Am. J. Pathol. 171, 1291–1303.

Spillantini, M.G., Crowther, R.A., Jakes, R., Cairns, N.J., Lantos, P.L., Goedert, M., 1998. Filamentous alpha-synuclein inclusions link multiple system atrophy with Parkinson's disease and dementia with Lewy bodies. Neurosci. Lett. 251 (3), 205–208.

Stefanova, N., Reindl, M., Neumann, M., Haass, C., Poewe, W., Kahle, P.J., et al., 2005. Oxidative stress in transgenic mice with oligodendroglial α-synuclein overexpression replicates the characteristic neuropathology of multiple system atrophy. Am. J. Pathol. 166, 869–876.

Stefanova, N., Reindl, M., Neumann, M., Kahle, P.J., Poewe, W., Wenning, G.K., 2007. Microglial activation mediates neurodegeneration related to oligodendroglial alpha-synucleinopathy: implications for multiple system atrophy. Mov. Disord. 22, 2196–2203. https://doi.org/10.1002/mds.21671.

Stefanova, N., Georgievska, B., Eriksson, H., Poewe, W., Wenning, G.K., 2012. Myeloperoxidase inhibition ameliorates multiple system atrophy-like degeneration in a transgenic mouse model. Neurotox. Res. 21, 393–404. https://doi.org/10.1007/s12640-011-9294-3.

Stemberger, S., Poewe, W., Wenning, G.K., Stefanova, N., 2010. Targeted overexpression of human α-synuclein in oligodendroglia induces lesions linked to MSA-like progressive autonomic failure. Exp. Neurol. 224, 459–464.

Strohäker, T., Jung, B.C., Liou, S.H., Fernandez, C.O., Riedel, D., Becker, S., et al., 2019. Structural heterogeneity of α-synuclein fibrils amplified from patient brain extracts. Nat. Commun. 10 (1), 5535. https://doi.org/10.1038/s41467-019-13564-w.

Sulzer, D., Alcalay, R.N., Garretti, F., Cote, L., Kanter, E., Agin-Liebes, J., et al., 2017. T cells from patients with Parkinson's disease recognize alpha-synuclein peptides. Nature. 546 (7660), 656–661. https://doi.org/10.1038/nature22815.

Takahashi, M., Tomizawa, K., Ishiguro, K., Sato, K., Omori, A., Sato, S., et al., 1991. A novel brain-specific 25 kDa protein (p25) is phosphorylated by a Ser/Thr-pro kinase (TPK II) from tau protein kinase fractions. FEBS Lett. 289, 37–43.

Tanji, K., Miki, Y., Mori, F., Nikaido, Y., Narita, H., Kakita, A., et al., 2019. A mouse model of adult-onset multiple system atrophy. Neurobiol. Dis. 127, 339–349. https://doi.org/10.1016/j.nbd.2019.03.020.

Tremblay, M.A., Acker, C.M., Davies, P., 2010. Tau phosphorylated at tyrosine 394 is found in Alzheimer's disease tangles and can be a product of the Abl-related kinase, Arg. J. Alzheimers Dis. 19 (2), 721–733. https://doi.org/10.3233/JAD-2010-1271.

Ubhi, K., Rockenstein, E., Mante, M., Inglis, C., Adame, A., Patrick, C., et al., 2010. Neurodegeneration in a transgenic mouse model of multiple system atrophy is associated with altered expression of Oligodendroglial-derived Neurotrophic factors. J. Neurosci. 30 (18), 6236–6246. https://doi.org/10.1523/JNEUROSCI.0567-10.2010.

Wang, F., Flanagan, J., Su, N., Wang, L.C., Bui, S., Nielson, A., et al., 2012. RNAscope: a novel in situ RNA analysis platform for formalin-fixed, paraffin-embedded tissues. J. Mol. Diagn. 14, 22–29. 22166544.

Watts, J.C., Giles, K., Oehler, A., Middleton, L., Dexter, D.T., Gentleman, S.M., et al., 2013. Transmission of multiple system atrophy prions to transgenic mice. Proc. Natl. Acad. Sci. U. S. A. 110 (48), 19555–19560.

Wenning, G.K., Stefanova, N., Jellinger, K.A., Poewe, W., 2008. Schlossmacher MG (2008) multiple system atrophy: a primary oligodendrogliopathy. Ann. Neurol. 64, 239–246.

West, M.J., Gundersen, H.J., 1990. Unbiased stereological estimation of the number of neurons in the human hippocampus. J. Comp. Neurol. 296, 1–22.

Williams, G.P., Marmion, D.J., Schonhoff, A.M., Jurkuvenaite, A., Won, W.J., Standaert, D.G., et al., 2020. T cell infiltration in both human multiple system

atrophy and a novel mouse model of the disease. Acta Neuropathol. https://doi.org/10.1007/s00401-020-02126-w.

Woerman, A.L., Kazmi, S.A., Patel, S., Freyman, Y., Oehler, A., Aoyagi, A., et al., 2018. MSA prions exhibit remarkable stability and resistance to inactivation. Acta Neuropathol. 135 (1), 49–63.

Yamasaki, R., Yamaguchi, H., Matsushita, T., Fujii, T., Hiwatashi, A., Kira, J.I., 2017. Early strong intrathecal inflammation in cerebellar type multiple system atrophy by cerebrospinal fluid cytokine/ chemokine profiles: a case control study. J. Neuroinflammation 14, 89. https://doi.org/10.1186/s12974-017-0863-0.

Yamasaki, T.R., Holmes, B.B., Furman, J.L., Dhavale, D.D., Su, B.W., Song, E.S., et al., 2019. Parkinson's disease and multiple system atrophy have distinct α-synuclein seed characteristics. J. Biol. Chem. 294 (3), 1045–1058. https://doi.org/10.1074/jbc.RA118.004471.

Yazawa, I., Giasson, B.I., Sasaki, R., Zhang, B., Joyce, S., Uryu, K., et al., 2005. Mouse model of multiple system atrophy α-synuclein expression in oligodendrocytes causes glial and neuronal degeneration. Neuron 45, 847–859.

Yoshida, M., 2007. Multiple system atrophy: alpha-synuclein and neuronal degeneration. Neuropathology 27 (5), 484–493.